Nd–Hf–O isotopic evidence for subduction-induced crustal replacement in NE China

3 authors, including:

Feng Guo
Chinese Academy of Sciences
117 PUBLICATIONS   **4,305** CITATIONS

Liang Zhao
Guangzhou Instutite of Geochemistry, Chinese Acadamy of Sciences
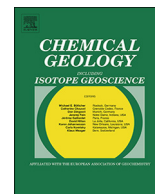**33** PUBLICATIONS   **660** CITATIONS

Some of the authors of this publication are also working on these related projects:

Mantle Geochemistry: Influence of plume on continental lithosphere View project

Superimposition of paleo-Pacific Subduction in ME China and its potential role in ore deposit formation View project

Nd-Hf-O isotopic evidence for subduction-induced crustal replacement in NE China

Feng Guo[a,b,*], Miwei Huang[a], Liang Zhao[a,b]

[a] State Key Laboratory of Isotope Geochemistry, Guangzhou Institute of Geochemistry, Chinese Academy of Sciences, Guangzhou 510640, China
[b] Institutions of Earth Science, Chinese Academy of Sciences, China

ABSTRACT

Convergent plate margins represent an ideal setting to understand the formation and evolution of the Earth's crust. Nevertheless, the geodynamic processes involved in crustal evolution remains highly debatable. Based on a large geochemical dataset of Permian-Cretaceous granitic rocks from the Yanbian area in NE China, we propose a new geodynamic model involving crustal replacement to decipher crustal evolution during a superimposed, multi-stage, subduction system. These Phanerozoic granitic rocks, from two adjacent zones, show contrasting Hf−Nd isotopic variation trends. With decreasing age of magmatism, whole-rock $\varepsilon_{Nd}(t)$ and zircon $\varepsilon_{Hf}(t)$ decrease gradually in the North Granite Zone (NGZ) but show the opposite trends in the South Granite Zone (SGZ). Zircon $\delta^{18}O$ shows a slight rise in the NGZ, but it initially increases from Permian to Jurassic and then decreases to Cretaceous in the SGZ. The Nd-Hf-O isotopic compositions of the Cretaceous granitic rocks in both zones converge. Four crustal components are identified in the source of granites across the Yanbian area, including (1) "juvenile" crust, (2) subduction-accretionary complex, (3) new arc crust, and (4) Precambrian crust.

The contributions made to the bulk crustal melting source of granites by the "juvenile" crust component in the NGZ and by the Precambrian crust in the SGZ were both gradually decreased, whereas the proportion of the new arc crust increased in both zones. Pre-existing crustal components were extensively eroded, destructed, diluted and replaced by the new arc crust formed during paleo-Pacific slab subduction. Considering the prevalence of these two Nd-Hf-O isotopic variation trends in many orogenic belts, subduction-induced crustal replacement represents an important mechanism for crustal evolution in convergent plate margins.

1. Introduction

The Earth's sialic crust makes it a unique planet in the solar system. Although debate remains about how this silicate crust is formed, most studies considered its majority to have formed in the early Earth's history, from Archean to early Proterozoic. Compared with this early crust, present-day continental crust is generally more evolved – with high concentrations of incompatible large ion lithophile elements (LILEs) and low contents of compatible elements, and evolved isotopic features (e.g., Rudnick and Gao, 2003). Several geodynamic processes at plate margins can strongly modify the chemical and isotopic compositions of the silicate crust. It can be recycled into mantle by plate subduction, and simultaneously be accreted to new crust through arc magmatism. The mafic eclogitic crust can be delaminated in response to gravitational instability (Kay and Kay, 1993; Gao et al., 2004), whereas intermediate-felsic rocks with negative buoyancy can be relocated in

the deep crust or even upper mantle through relamination (Hacker et al., 2011). Nevertheless, the precise role that such processes take in crustal evolution remains highly debatable, particularly in the case of convergent plate margin settings, where the interaction of multiple crustal evolution processes is probably the most complicated.

On one hand, convergent plate margins incorporate multiple crustal components, including subducted oceanic crust, overlying sediment, subduction-accretionary complex, pre-existent continental crust and newly formed arc crust. On the other hand, the range of mechanisms through which these components may interact to form new hybrid crust is intensive (Voshage et al., 1990; Kay and Kay, 1993; von Huene et al., 2004; Hacker et al., 2011). These complexities make it difficult to quantitatively evaluate the respective contribution of each crustal component. However, since convergent plate margins form one of the most important sites to decipher the Earth's crustal growth and re-working, the geodynamic processes that operate at these margins are of

crucial significance in understanding the crust-mantle interaction and mass recycling of the Earth.

One powerful approach to investigating crustal evolution is by integrating studies of zircon U-Pb-Hf-O and whole-rock Nd isotopes of granite (e.g., Kemp et al., 2006, 2009; Vervoort and Kemp, 2016). Although some intraplate A-type granites and plagiogranites in ophiolitic suite are probably mantle-derived, the majority of granitic rocks are formed through melting of crustal protoliths. The whole-rock Nd isotope data of granite reflect the average residual age and composition of its crustal protoliths (DePaolo, 1981). "Juvenile" crust is characterized by highly radiogenic Nd isotopic composition, with a depleted mantle model age (T_{DM}) close to its formation time (e.g., DePaolo, 1981; Jahn et al., 2000). In contrast, recycled crust has a less radiogenic Nd composition and a T_{DM} significantly older than the crystallization age. In addition to whole-rock Nd isotope data, zircon Hf−O isotopic compositions can clearly record the crustal growth and reworking processes (Valley, 2003; Hawkesworth and Kemp, 2006; Kemp et al., 2006; Vervoort and Kemp, 2016). If the spatial and temporal Nd-Hf-O isotopic variations of the granitic rocks reflect the compositional and isotopic changes of the bulk crustal source, then the crustal evolution can be reconstructed through Hf-Nd-O isotope analyses on the granites of different ages.

The Yanbian area is located at the junction of China, Russia and Korea, an important part of the Northeast Asian continental margin. This area is also a joint between the Central Asian Orogenic Belt (CAOB) and North China Craton (NCC). The CAOB consists mainly of subduction-accretionary complex of "juvenile" nature in terms of Nd and Hf isotopes (e.g., Sengör et al., 1993; Jahn et al., 2000; Wu et al., 2000; Xiao et al., 2003; Yang et al., 2006; Guo et al., 2010). By contrast, the NCC is one of the oldest cratons on Earth and comprise predominantly Archean to early Proterozoic metamorphic rocks with non-radiogenic Nd and Hf isotopic compositions (e.g., Geng et al., 2012; Liu et al., 2014). The Yanbian area has witnessed a multi-stage history of oceanic slab subduction, including the Paleozoic subduction of the paleo-Asian Ocean, the Mesozoic subduction of the paleo-Pacific Ocean, and the Cenozoic subduction of the Pacific Ocean (e.g., Guo et al., 2007, 2015, 2016; Wu et al., 2011; Xu et al., 2013; Zhang et al., 2016). It is, therefore, an ideal site to investigate the crustal growth and reworking processes superimposed by multi-stage subduction systems. In this paper, we present a large geochemical dataset, including the whole-rock major, trace element, Nd isotopic compositions and in-situ zircon U−Pb ages and Hf−O isotopic compositions of granitic rocks from the Yanbian area emplaced from Permian to Cretaceous. These new data, together with previous age and isotopic data from related mafic rocks (Yu et al., 2012; Guo et al., 2015, 2016; Zhao et al., 2019), enables us to identify the possible crustal components that have been involved in the melting source, and to further estimate the proportions of crustal growth attributable to subduction of the paleo-Asian and paleo-Pacific Oceans. Based on the spatial-temporal variation of crustal components in the melting source, we propose a new geodynamic model that invokes a process of crustal replacement as the primary driver of crustal evolution in the Northeast Asian continental margin.

2. Geological backgrounds

Northeast Asia comprises a series of subduction-related accretionary orogens distributing among the NCC, Siberian Craton and the Pacific Plate (Fig. 1a, Maruyama et al., 1989; Tang, 1990; Sengör et al., 1993; Xiao et al., 2003). The history of tectonic evolution includes: (1) subduction and accretion of the paleo-Asian Ocean during Paleozoic to form the giant CAOB; and (2) northwestward subduction and accretion of the paleo-Pacific Plate to the Eurasia Continent, thereby controlling the evolution of the Northeast Asian continental margin since the Mesozoic (Maruyama et al., 1989; Guo et al., 2007; Wu et al., 2011).

The Yanbian area is in the eastern CAOB. Phanerozoic granitic rocks are widely exposed over an area of > 20,000 km^2 and occupy ~70% of the region (Fig. 1b). The emplacement of these granites occurred from late Paleozoic (291 Ma) to early Cretaceous (112 Ma), but predominantly between 210 and 155 Ma (Zhang et al., 2004; Wu et al., 2011). In addition, extensive eruption of predominant intermediate-felsic lavas also occurred from late Triassic to early Cretaceous (228–106 Ma) (Li et al., 2007; Xu et al., 2009). Compared with the voluminous granitic rocks and their eruptive counterparts, Phanerozoic (Permian to early Jurassic) mafic intrusions are only sporadically distributed in the Yanbian area and its adjacent regions (Yu et al., 2012; Guo et al., 2015, 2016; Zhao et al., 2019).

The Phanerozoic granitic rocks were collected from both sides of the Fu'erhe- Gudonghe Fault (Fig. 1b), which has widely been considered as a boundary between the NCC and CAOB in the easternmost segment (e.g., Jia et al., 2004; Li et al., 2010a). To facilitate the discussion of these granitic rocks and their petrogenesis, we have divided them spatially into those located northeast of the fault [hereafter the North Granite Zone (NGZ)] and those southwest of the fault [hereafter the South Granite Zone (SGZ)] (Fig. 1b). The rock types in the SGZ include tonalite, quartz diorite, granodiorite, garnet-bearing granite and monzogranite (Fig. S1-1). In the NGZ, they include tonalite, quartz diorite, granodiorite, trondhjemite, monzogranite and syenogranite (Fig. S1-2). Age data relating to the granites are mainly based on the literature summarized by Wu et al. (2011), however, we complement this with new zircon U−Pb ages of eleven samples either from previously undated felsic intrusions or from samples having existing ages with relatively large analytical uncertainties (Fig. 2).

Sampling locations, detailed petrographic description, mineral compositions and zircon U−Pb ages of 33 granitic plutons (37 samples) from the Yanbian area are summarized in Table 1.

3. Analytical techniques

3.1. Zircon U-Pb-Hf-O isotope analyses

Zircon grains were separated and concentrated from the rock samples using the conventional heavy liquid and magnetic techniques and purified by handpicking under a binocular microscope. After being mounted in epoxy resin, the zircon grains were polished to approximately half crystal width, then coated with gold and examined for internal textures using the cathodoluminescence (CL) images. Typical CL images of zircon from the granitic samples are presented in Fig. S2.

Zircon U−Pb dating was performed at the Guangzhou Institute of Geochemistry (GIG), Chinese Academy of Sciences (CAS). The isotope and trace element compositions of zircon were measured in-situ by laser ablation inductively coupled plasma mass spectrometry (LA-ICP-MS). Laser ablation was accomplished using a pulsed Resonetic 193 nm ArF excimer laser, operated at a constant energy of 80 mJ, with a repetition rate of 8 Hz and a spot diameter of 30 μm (Li et al., 2012b). Helium gas carrying the ablated sample aerosol is mixed with argon carrier gas and nitrogen as additional di-atomic gas to enhance sensitivity, and finally flows into ICP-MS. Prior to analysis, the LA-ICP-MS system was optimized using NIST SRM610 ablated with 30 μm spot size and 5 μm/s scanning speed to achieve maximum signal intensity and low oxide rates. Each analysis included approximately 20–30 s of background acquisition (from a gas blank) followed by 50 s of data acquisition from the sample. Temora-1 zircon (417 Ma, Black et al., 2003) was used as the primary standard and Qinghu zircon (159 Ma, Li et al., 2009) as the secondary standard to calibrate the U−Pb age of zircon. The reference material (NIST SRM610) was used as external calibration reference and Si was used as the internal standard to quantify elemental concentrations in zircon. The off-line selection and integration of the background and analyte signals, time-drift correction and quantitative calibration, were performed using ICPMSDataCal (Liu et al., 2008). Isotopic ratios and concentrations were calculated by the GLITTER program. Common Pb correction was processed with non-radiogenic ^{204}Pb, following the method of Anderson (2002). The weighted mean U−Pb age and
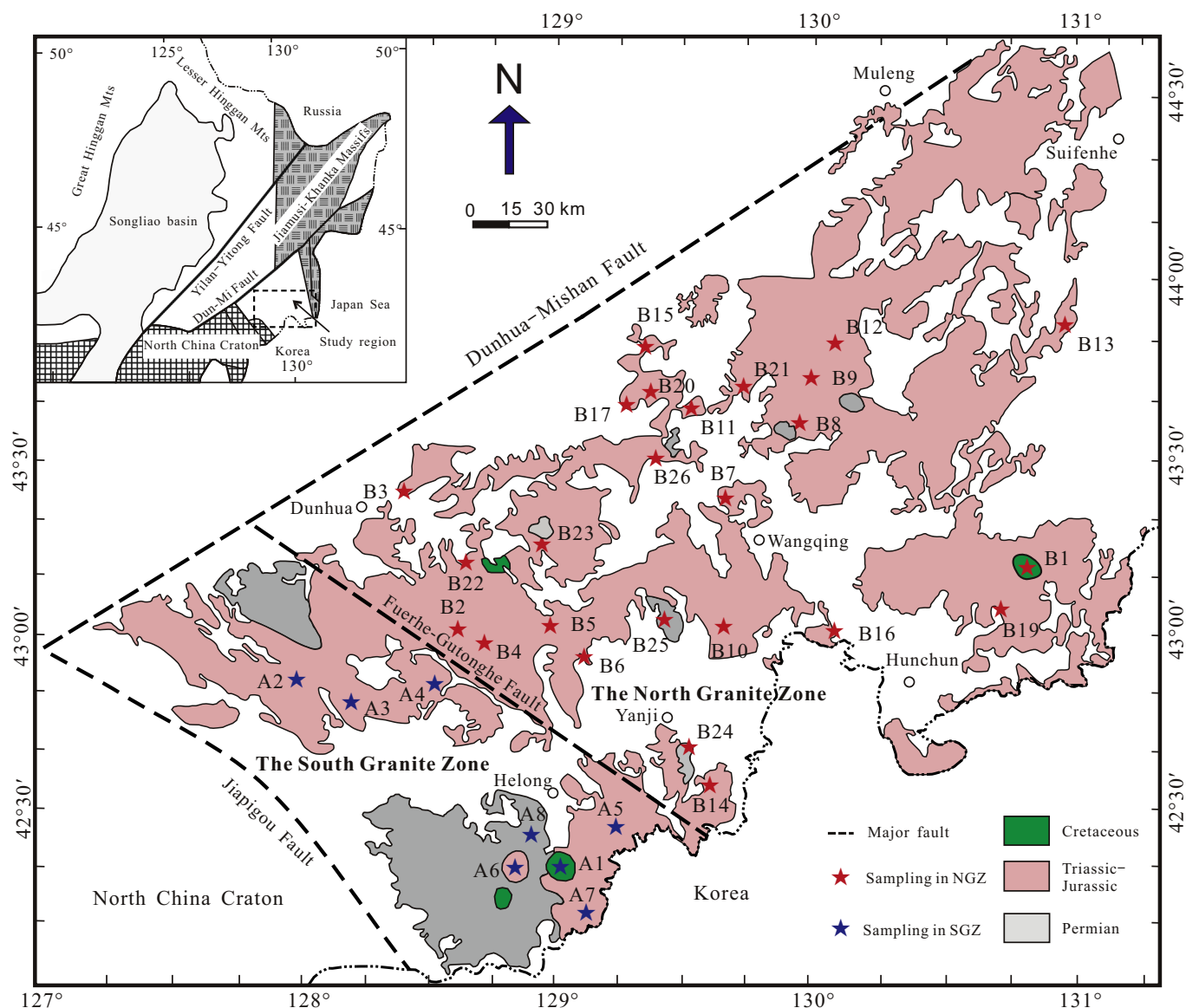
Fig. 1. A simplified map showing the tectonic units in NE China [a, modified after Wu et al., 2000 and Guo et al., 2007] and distribution of Permian-Cretaceous granites from the Yanbian area, NE China (b).

Concordia plots were obtained using ISOPLOT (version 3.0, Ludwig, 2003). The zircon U−Pb age, analytical uncertainty and data report follow the methods recommended in Košler et al. (2013), Horstwood et al. (2016) and Spencer et al. (2016). The analytical results and U−Pb ages of zircon from eleven Phanerozoic granitic plutons in the Yanbian area are listed in Table S1 and illustrated in Fig. 2.

Zircon Lu–Hf isotopic analyses were conducted on a Neptune multiple collector ICP-MS (MC-ICP-MS) equipped with 193 nm ArF excimer laser-ablation system at the Institute of Geology and Geophysics (IGG), CAS. A laser repetition rate of 8 Hz at 100 mJ was used in this study, with ablation spots of 44 μm in diameter. The detailed analytical procedures were followed those described by Wu et al. (2006) and Xie et al. (2008). The methods of isobaric interference (e.g., from ^{176}Lu or ^{176}Yb on ^{176}Hf) correction, with a range from low to high Yb/Hf and Lu/Hf ratios, can be found in Wu et al. (2006) and Fisher et al. (2011). During the analysis, the raw count rates for ^{172}Yb, ^{173}Yb, ^{175}Lu, ^{176} (Hf + Yb + Lu), ^{177}Hf, ^{178}Hf, ^{179}Hf and ^{180}Hf were collected. The working conditions for the instrument were monitored by the stable isotope ratios of ^{180}Hf/^{177}Hf, which is constant at around 1.8867. ^{175}Lu was used for interference correction of ^{176}Lu on ^{176}Hf. The

^{176}Yb/^{172}Yb value of 0.5887 and mean β$_{Yb}$ value obtained during Hf analysis on the same spot were applied for the interference correction of ^{176}Yb on ^{176}Hf (Wu et al., 2006). The determined ^{176}Hf/^{177}Hf and ^{176}Lu/^{177}Hf ratios of the Mud Tank standard zircon were 0.282499 ± 5 (2σ, n = 56) and 0.000048, the GJ-1 standard zircon were 0.282020 ± 5 (2σ, n = 56) and 0.00027, and those for the Temora standard zircon were 0.282685 ± 32 (2σ, n = 12) and 0.0011. These ratios were in good agreement within errors with the recommended ^{176}Hf/^{177}Hf values of 0.282504 ± 44 for Mud Tank and 0.282015 ± 19 for GJ-1 and 0.282685 ± 8 for Temora (Woodhead and Hergt, 2005). The Lu−Hf isotopic compositions of zircon from the Phanerozoic granitic rocks and analytical results of zircon standards (GJ-1, Mud Tank and Temora) are listed in Table S2.

In-situ zircon oxygen isotopic analyses were conducted using a Secondary Ion Mass Spectrometry (SIMS) Cameca ims-1280 at the IGGCAS. The Cs$^+$ primary beam was accelerated at 10 kV with an intensity of ca. 2 nA and rastered over a 10 μm area. The spot size was about 20 μm in diameter (10 μm beam diameter + 10 μm raster). An electron gun was used to compensate for sample charging during analysis. Secondary ions were extracted with a − 10 kV potential. Oxygen
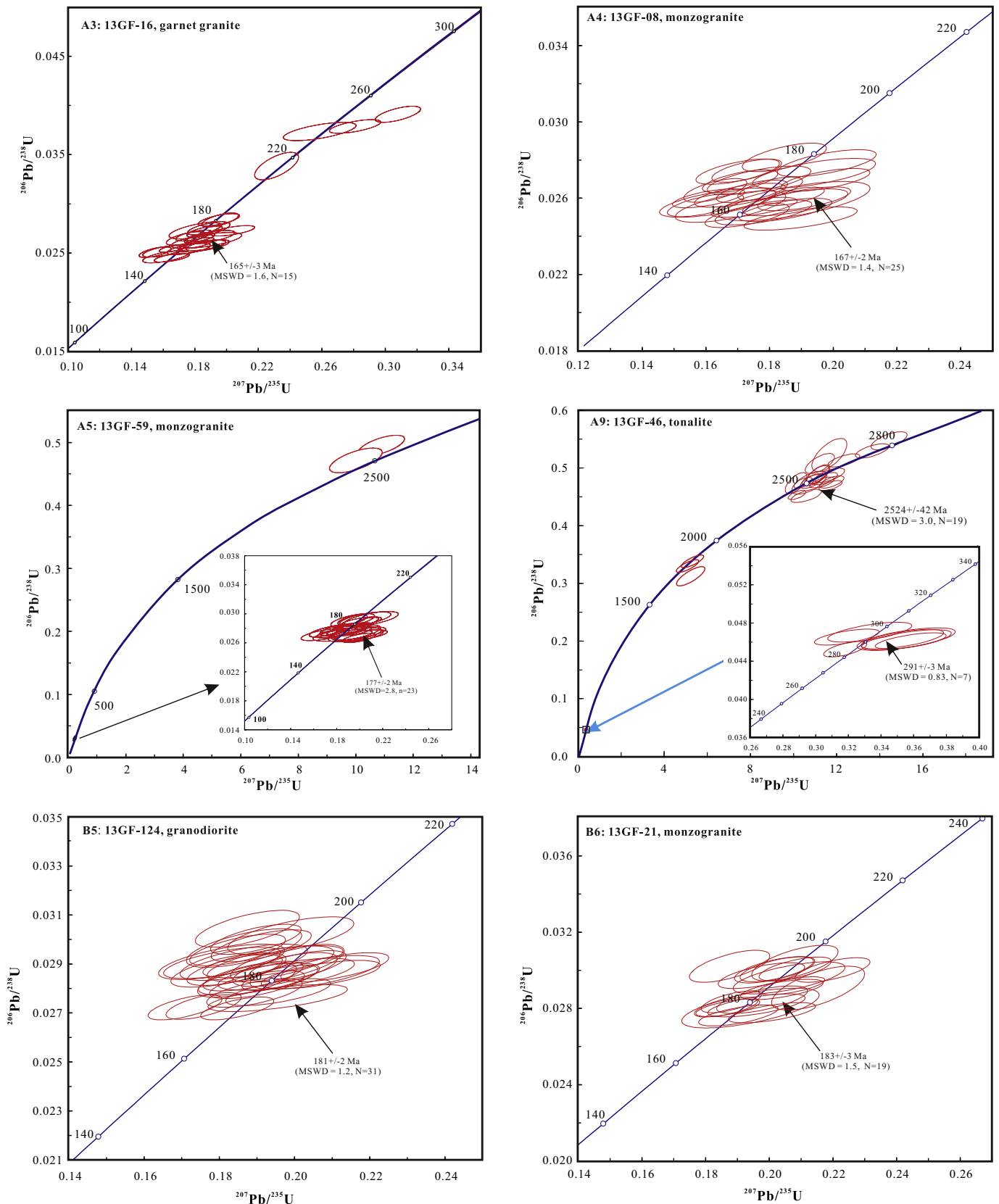
Fig. 2. New zircon U−Pb dating results of eleven samples of granitic plutons in the Yanbian area, NE China.

isotopes were measured in multi-collector mode with two off-axis Faraday cups with each analysis consisting of 4 × 20 cycles of ion counting. The O isotope results are reported in the conventional δ18O

notation relative to the reference standard VSMOW. The instrumental mass fractionation factor (IMF) was corrected using the zircon standard 91,500 with δ18O = 9.9‰ (Wiedenbeck et al., 2004). External

Table 1
Summary of the Phanerozoic granitoid plutons in the Yanbian area, NE China.

Sample	Pluton No	Locality	Geographic coordinates	Age (Ma)	Rock type	Mineral assemblage	Whole-rock $\varepsilon_{Nd}(t)$	Zircon $\varepsilon_{Hf}(t)$	Zircon $\delta^{18}O$ (‰)
The South Granite zone (SGZ)									
13GF-40	A1	Liudong	42°18′29″N, 128°02′09″E	114 ± 2	Monzogranite	Hb + Bi + Kf + Pl + Qz	−2.5	3.0 ± 0.7	6.01 ± 0.11
13GF-19	A2	Dakai	42°52′29″N, 128°30′25″E	159 ± 5	Monzogranite	Hb + Bi + Kf + Pl + Qz	−4.3	2.0 ± 0.4	8.82 ± 0.30
13GF-16*	A3	Dongqing	42°48′30″N, 128°13′37″E	165 ± 3	Garnet granite	Grt + Bi + Kf + Pl + Qz	−1.8	4.6 ± 1.0	7.89 ± 0.60
13GF-08*	A4	Huangniling	42°52′29″N, 128°02′15″E	167 ± 3	Monzogranite	Hb + Bi + Kf + Pl + Qz	−1.9	4.0 ± 1.2	7.57 ± 0.30
13GF-05				168 ± 3	Granodiorite		−3.3	3.0 ± 1.2	7.98 ± 0.39
13GF-59*	A5	Shacongdingzi	42°31′39″N, 129°05′41″E	177 ± 2	Monzogranite	Hb + Bi + Kf + Pl + Qz	−5.6	1.7 ± 1.0	6.13 ± 0.23
13GF-48	A6	Bailiping	42°12′42″N, 129°49′21″E	245 ± 6	Monzogranite	Hb + Bi + Kf + Pl + Qz	−8.1	−8.3 ± 1.3	7.57 ± 0.30
13GF-50			42°20′21″N, 129°50′19″E	245 ± 6	Granodiorite	Hb + Bi + Kf + Pl + Qz		−9.1 ± 1.9	7.39 ± 0.46
13GF-42	A7	Nanping	42°11′00″N, 129°09′21″E	246 ± 3	Quartz diorite	Hb + Bi + Kf + Pl + Qz	−8.2	−9.6 ± 0.5	7.15 ± 0.31
13GF-46*	A8	Shiliping	42°28′44″N, 129°56′57″E	291 ± 3	Tonalite	Hb + Bi + Kf + Pl + Qz	−13.4	−18.7 ± 2.3	5.78 ± 0.36
The North Granite Zone (NGZ)									
13GF-83	B1	Xiaoxinancha	43°08′14″N, 130°50′02″E	112 ± 1	Tonalite	Hb + Bi + Kf + Pl + Qz	0.9	8.2 ± 0.4	5.85 ± 0.34
13GF-3	B2	Changle	42°24′08″N, 128°24′27″E	179 ± 1	Monzogranite	Hb + Bi + Kf + Pl + Qz	2.6	8.9 ± 0.5	5.20 ± 0.43
13GF-31	B3	Mengshan	42°53′05″N, 128°46′08″E	181 ± 2	Monzogranite	Hb + Bi + Kf + Pl + Qz	1.2	6.7 ± 0.5	6.12 ± 0.36
13GF-36	B4	Shimen	43°02′31″N, 128°59′26″E	182 ± 2	Granodiorite	Hb + Bi + Kf + Pl + Qz	0	8.3 ± 0.7	5.58 ± 0.32
13GF-124*	B5	Liucun	43°07′39″N, 129°30′36″E	182 ± 2	Granodiorite	Hb + Bi + Kf + Pl + Qz	2.8	8.1 ± 0.6	6.05 ± 0.08
13GF-21*	B6	Xinhe	42°52′29″N, 128°30′25″E	183 ± 3	Monzogranite	Hb + Bi + Kf + Pl + Qz	2.2	9.9 ± 0.5	5.30 ± 0.32
13GF-70*	B7	Qingmingtun	43°07′39″N, 129°30′36″E	184 ± 3	Monzogranite	Hb + Bi + Kf + Pl + Qz	3.1	8.5 ± 0.7	5.72 ± 0.36
13GF-39	B8	Yushuchuan	42°59′02″N, 128°06′18″E	186 ± 1	Monzogranite	Hb + Bi + Kf + Pl + Qz	2.0	9.6 ± 0.9	6.06 ± 0.36
13GF-107*	B9	Daxinggou	43°23′53″N, 129°39′17″E	187 ± 1	Granodiorite	Hb + Bi + Kf + Pl + Qz	2.8	7.4 ± 0.4	6.11 ± 0.29
13GF-110	B10	Dadingzi	43°35′50″N, 129°56′17″E	189 ± 3	Granodiorite	Hb + Bi + Kf + Pl + Qz	2.2	8.0 ± 0.4	5.66 ± 0.35
13GF-126	B11	Miantuian	43°02′09″N, 129°38′45″E	189 ± 1	Granodiorite	Hb + Bi + Kf + Pl + Qz	2.9	9.1 ± 0.3	5.86 ± 0.38
13GF-101	B12	Luotuoshan	43°38′45″N, 129°32′09″E	190 ± 2	Monzogranite	Hb + Bi + Kf + Pl + Qz	2.9	8.9 ± 0.5	5.25 ± 0.37
13GF-113	B13	Xidahe	43°47′56″N, 130°13′07″E	195 ± 3	Granodiorite	Hb + Bi + Kf + Pl + Qz	1.9	7.2 ± 0.4	6.16 ± 0.36
13GF-115								7.8 ± 0.5	6.29 ± 0.27
13GF-79	B14	Naozhi	43°53′09″N,130°58′14″E	196 ± 3	Monzogranite	Hb + Bi + Kf + Pl + Qz	3.0	10.0 ± 0.5	4.11 ± 0.38
13GF-69	B15	Tianfozishan	129°37′06″N,42°34′35″E	196 ± 7	Monzogranite	Hb + Bi + Kf + Pl + Qz	0.9	8.4 ± 0.8	6.15 ± 0.29
13GF-89	B16	Laosongling	43°49′39″N,129°29′56″E	197 ± 2	Monzogranite	Hb + Bi + Kf + Pl + Qz	2.4	6.4 ± 1.0	6.32 ± 0.39
13GF-117*	B17	Luozigou	43°42′36″N,130°22′31″E	204 ± 2	Monzogranite	Hb + Bi + Kf + Pl + Qz	3.3	9.2 ± 0.6	5.05 ± 0.10
13GF-91	B18	Chunyang	43°42′05″N,129°21′51″E	205 ± 1	Syenogranite	Hb + Bi + Kf + Qz	2.3	7.8 ± 0.6	6.16 ± 0.37
13GF-85	B19	Sandaogou	43°05′08″N,130°43′59″E	205 ± 1	Monzogranite	Hb + Bi + Kf + Pl + Qz	3.2	10.2 ± 0.6	5.51 ± 0.32
13GF-87			43°05′08″N,130°43′59″E	205 ± 1	Syenogranite	Hb + Bi + Kf + Qz	3.7	8.5 ± 1.3	5.48 ± 0.33
13GF-93	B20	Chunyang	43°42′13″N,129°25′29″E	215 ± 5	Monzogranite	Hb + Bi + Kf + Pl + Qz	2.0	8.7 ± 0.8	6.38 ± 0.39
13GF-77*	B21	Liangshuizhen	42°58′10″N,130°03′09″E	215 ± 2	Quartz diorite	Hb + Bi + Kf + Pl + Qz	4.2	11.0 ± 0.6	5.53 ± 0.36
13GF-104	B22	Shenxiandong	43°43′01″N,129°44′14″E	218 ± 2	Syenogranite	Hb + Bi + Kf + Qz	3.9	9.6 ± 0.5	4.73 ± 0.39
13GF-32	B23	Jianchanggou	43°16′27″N,128°45′36″E	228 ± 2	Syenogranite	Hb + Bi + Kf + Qz	2.3	8.9 ± 0.6	4.94 ± 0.31
13GF-111*	B24	Huapidianzi	43°39′57″N,130°04′24″E	260 ± 3	Plagiogranite	Hb + Bi + Pl + Qz	3.3	9.9 ± 0.9	5.24 ± 0.18
13GF-105	B25	Hongshitun	43°29′35″N,129°23′54″E	266 ± 2	Syenogranite	Hb + Bi + Kf + Qz	3.8	9.7 ± 1.0	4.80 ± 0.36

Mineral abbreviations: Hb – hornblende; Bi – biotite; Kf – K-feldspar; Pl – plagioclase; Grt – garnet; Qz - quartz.

Note: All zircon Hf and O isotopic compositions are analyzed in this study. The whole-rock Nd isotopic compositions are from Huang et al. (2015) and references therein. The zircon U−Pb ages are compiled from Wu et al. (2011) and references therein. Additional zircon U−Pb age analyses were conducted for those samples marked with "*" in the upright with the zircon U−Pb isotope data listed in Table S1.

reproducibility of the zircon standards was typically better than 0.4‰ (2σ) for $\delta^{18}O$. Detailed description of the analytical procedure was reported in Li et al. (2010a, 2010b) and Guo et al. (2014). During analysis, the Penglai zircon standard yields $\delta^{18}O$ = 5.30 ± 0.11‰ (n = 150) and the Qinghu zircon standard gives $\delta^{18}O$ = 5.43 ± 0.15‰ (n = 100). The in-situ zircon O isotopic compositions of 37 Phanerozoic granitic samples are also listed in Table S2.

3.2. Whole-rock elemental and Nd isotopic analyses

Representative samples selected for whole-rock elemental and Nd isotopic analyses were crushed to millimeter-sized chips after removing weathered rims, washed in 0.05 N HCl and cleaned with de-ionized water. The chips were crushed to < 20 mesh in a corundum crusher and then ground to < 200 mesh in an agate ring mill. Whole-rock major element analyses were performed at the GIGCAS, using an X-ray fluorescence spectrometry with analytical errors < 2%. Trace elements were analyzed at the Institute of Geochemistry, CAS by a Finnigan ICP-MS. Approximately 100 mg of powder was dissolved in HF and HNO3 at 190 °C for 12 h in screw-top PTFE-lined stainless steel bombs during pretreatment. Analytical precision for rare earth elements (REE) and high field strength elements (HFSE) is estimated to be 5% and for other elements about 10% (Qi et al., 2000). The major oxide and trace element analytical results for international standards are reported in Table S3.

Neodymium isotopic analyses were performed at the GIGCAS by a Micromass Isoprobe MC-ICP-MS. The detailed analytical procedure was described in Liang et al. (2003). Repeated analyses on the Nd isotope standard JNdi-1 yield $^{143}Nd/^{144}Nd$ = 0.512115 ± 4 (2σ, n = 8), consistent with its certified value ($^{143}Nd/^{144}Nd$ = 0.512115 ± 7, Tanaka et al., 2000). Neodymium isotopic ratios were normalized to $^{146}Nd/^{144}Nd$ = 0.7219. During the Nd isotope analysis, eight analyses of rock standard BHVO-2 and JB-3 gave $^{143}Nd/^{144}Nd$ = 0.512967 ± 6 (2σ, n = 8) and $^{143}Nd/^{144}Nd$ = 0.513045 ± 6 (2σ, n = 8), respectively. The procedure blank for Nd was ~50 pg. The whole-rock major and trace element compositions and Nd isotopic results are presented in Table S4.

During the calibration of initial whole-rock Nd and zircon Hf isotope compositions of the analyzed samples, the selected Nd and Hf isotope ratios of chondrite and depleted mantle (DM) were those reported in Bouvier et al. (2008) and Chauvel et al. (2014). The whole-rock Nd isotope data and average zircon Hf−O isotopic compositions of the Yanbian granitic rocks are also summarized in Table 1.
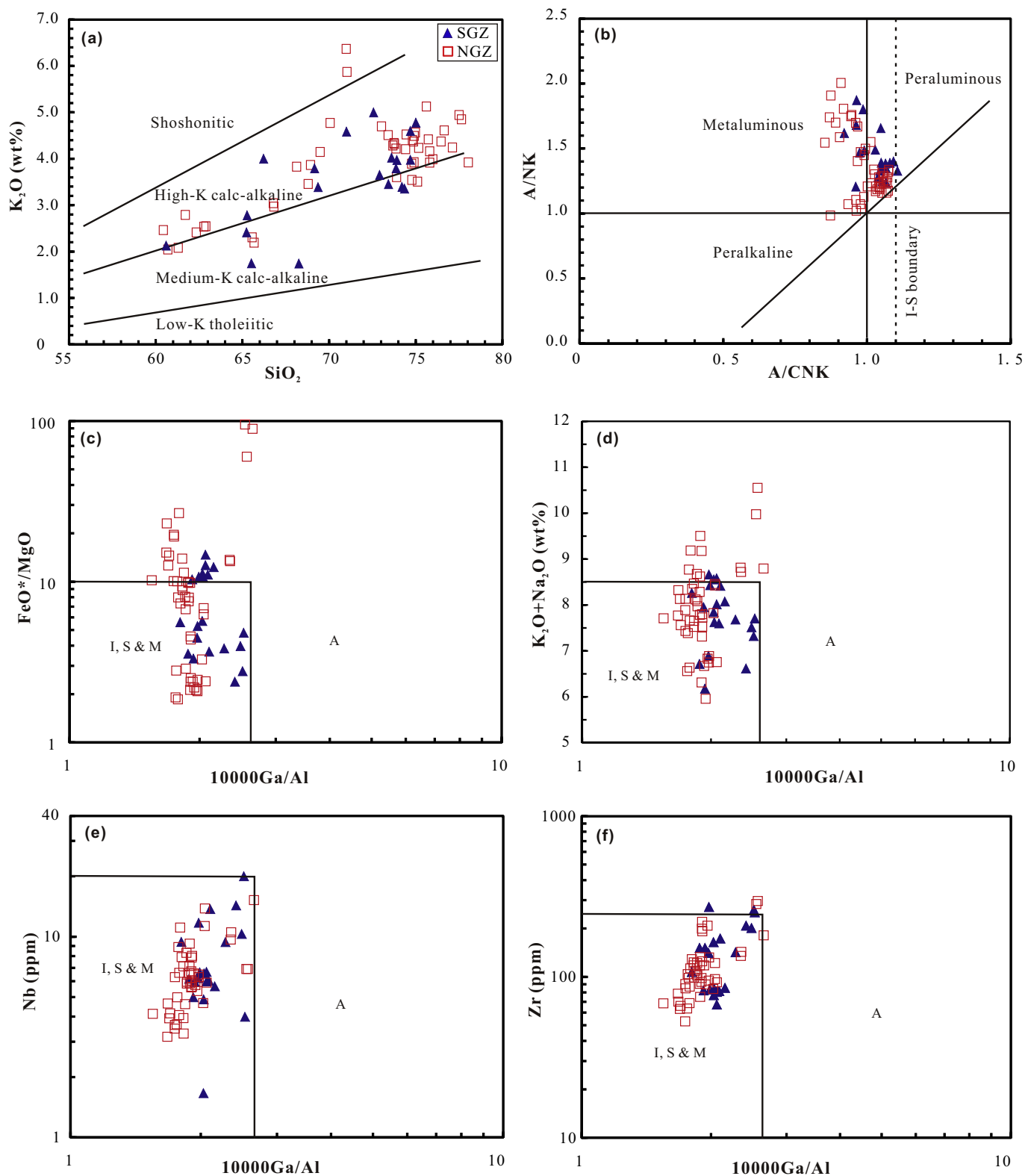
Fig. 3. (a) K_2O vs. SiO_2, (b) A/CNK vs. A/NK, and (c) FeO*/MgO, (d) $K_2O + Na_2O$, (e) Nb, (f) Zr vs. 10000Ga/Al classification diagrams (Whalen et al., 1987), indicating that the Yanbian granitic rocks are predominantly calc-alkaline, metaluminous I-type granites. A/NK = $Al_2O_3/(Na_2O + K_2O)$, A/CNK = $Al_2O_3/(Na_2O + K_2O + CaO)$ in molecular ratio; FeO* refers to total iron oxides. A few samples with extremely high FeO*/MgO ratios are highly fractionated granites.
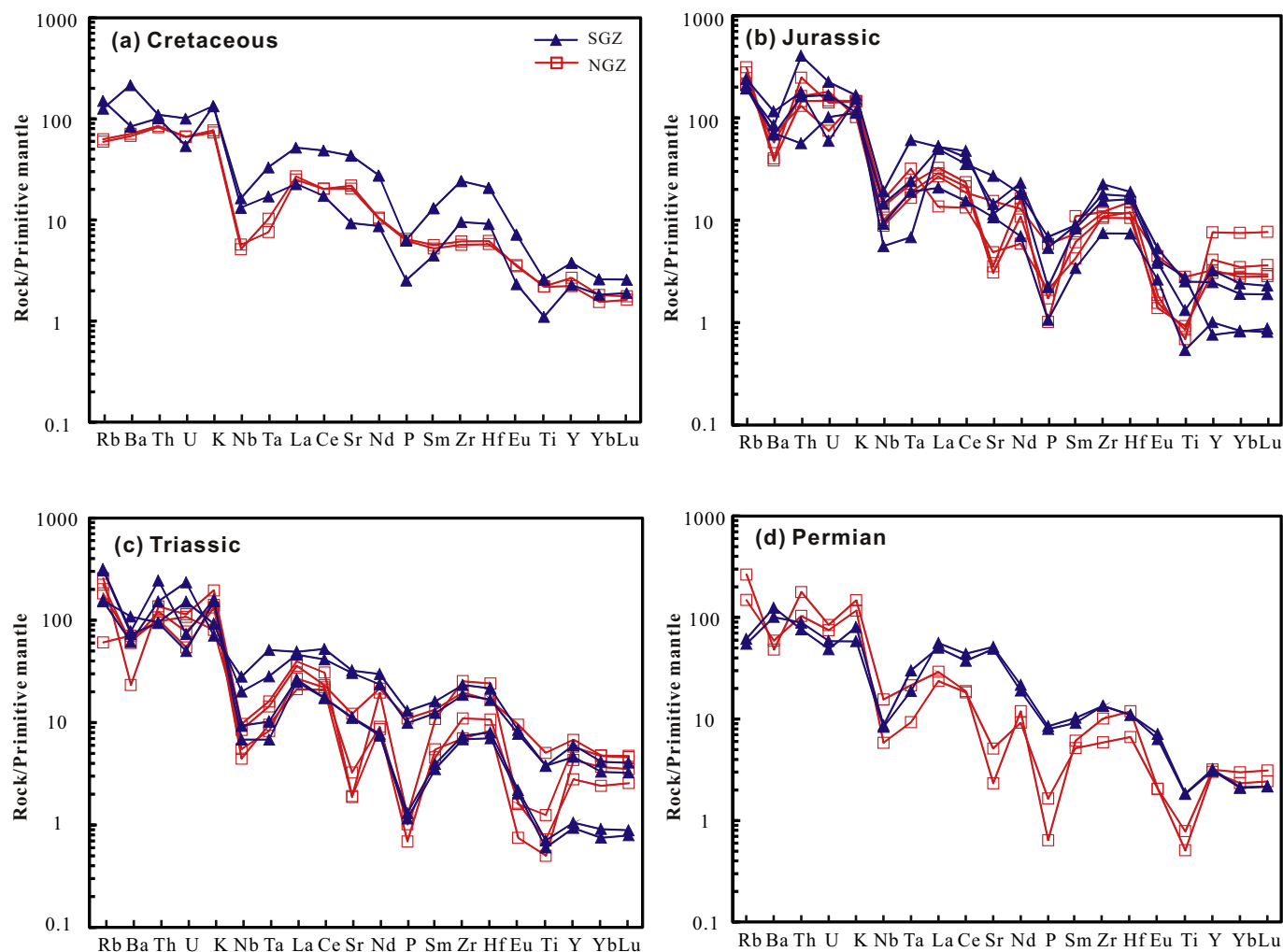
Fig. 4. Primitive mantle-normalized trace element spidergrams of representative samples of Phanerozoic granitic rocks in the Yanbian area, NE China. Normalization values for trace elements are from Sun and McDonough (1989).

4. Results

4.1. Compositional variations of the Phanerozoic granites

The Permian to Cretaceous granitic rocks span a large range in SiO$_2$ (60.4–78.0%) and MgO (0.02–3.13%). They have a K$_2$O range between 1.74 and 6.37%, and most of them are medium-K to high-K calc-alkaline with minor shoshonitic examples (Fig. 3a). These rocks are metaluminous to peraluminous (Fig. 3b), spanning a range of A/CNK [Al$_2$O$_3$/(CaO + Na$_2$O + K$_2$O) in molar ratio] from 0.77 to 1.11. In the granite classification diagrams of Whalen et al. (1987), they span the fields for I-, S- and M-type instead of A-type granite (Fig. 3c-f), although the generally metaluminous and K-rich compositions suggest that the Phanerozoic Yanbian granitic rocks are I-type (Fig. 3).

The granites generally show right-declined chondrite-normalized REE patterns, with (La/Yb)$_N$ ratios (the subscript 'N' denotes chondrite normalization) between 2 and 61 and a Eu/Eu* range of 0.15–0.94 (Table S4 and Fig. S3). All samples show enrichment in LILEs such as Rb, Ba, K and LREEs, but depletion in high field strength elements (HFSEs) and HREEs (Fig. 4). Some granitic rocks (e.g., the Permian tonalite in the SGZ and the Cretaceous tonalite and granodiorite in both zones) show adakitic trace element geochemistry including high Sr (> 400 ppm) and low Y concentrations (< 18 ppm) and high Sr/Y ratios (Table S4 and Fig. 4). The granites in the SGZ generally have higher Sr/Y, (La/Yb)$_N$, Eu/Eu* and lower Rb/Sr ratios than those in the NGZ

(Fig. 5). The higher Rb/Sr and lower Eu/Eu* ratios in the NGZ granites indicate higher degrees of differentiation, whereas the higher Sr/Y and (La/Yb)$_N$ ratios in the SGZ granites suggest either high-pressure melting conditions or are features inherited from their protoliths (Ma et al., 2015).

4.2. Nd-Hf-O isotopic variations of the Phanerozoic granites

4.2.1. The South Granite Zone

The Phanerozoic granitic rocks in the SGZ span an emplacement age between 291 and 114 Ma (Table 1, Zhang et al., 2004; Wu et al., 2011). The early Permian Shiliping pluton consists of tonalite. It has highly negative whole-rock ε$_{Nd}$(t) of −13.4 and also highly negative zircon ε$_{Hf}$(t) between −26.1 and −14.8 (Tables S2 and S4, Zhang et al., 2004). However, the magmatic zircon has mantle-like δ^{18}O value between 5.4 and 6.5‰ (Table S2, Valley, 2003). In addition, there exists abundant inherited zircon with Archean to early Proterozoic ages (Table S1 and Fig. 2). These zircon grains also develop highly non-radiogenic Hf (ε$_{Hf}$(0) = −58.5 to −37.4) and span a similar δ^{18}O (5.2–6.6‰) range to the magmatic zircon (Table S2).

The Triassic granitic rocks include quartz diorite, granodiorite and monzogranite. They also have negative whole-rock ε$_{Nd}$(t) values of around −8.0 (Table 1). Most (~97%) analyzed zircon grains show negative ε$_{Hf}$(t) value from −16.4 to −0.1, with only 1.5% of zircon having ε$_{Hf}$(t) > 0 (Fig. 6). Nearly two thirds (62%) of the magmatic
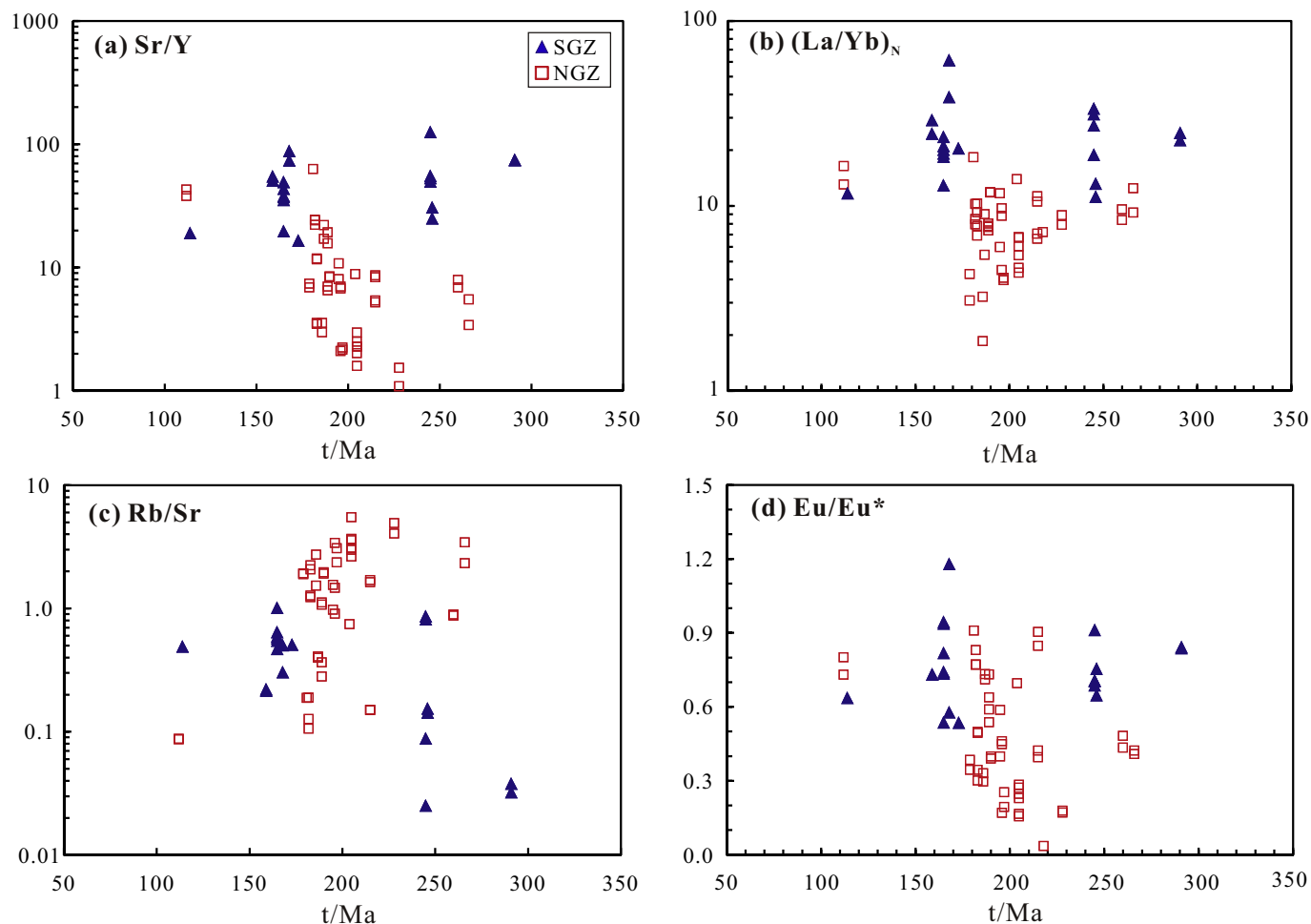
Fig. 5. Sr/Y, (La/Yb)$_N$, Rb/Sr and Eu/Eu* ratios versus emplacement age (Ma) of Permian-Cretaceous granitic rocks from the Yanbian area, NE China. The subscript "N" denotes normalization by chondrite. The trace element values of chondrite are from Taylor and McLennan (1985).

zircon have $\delta^{18}O > 7.0‰$ (Fig. 8), which is much higher than the range of $\delta^{18}O$ for mantle-derived zircon. The Triassic granites clearly have higher whole-rock $\varepsilon_{Nd}(t)$ and zircon $\varepsilon_{Hf}(t)$ and $\delta^{18}O$ values than the Permian tonalite.

The Jurassic felsic plutons include granodiorite, monzogranite and garnet-bearing granite. They also show negative whole-rock $\varepsilon_{Nd}(t)$ between -5.6 and -1.8, but the majority (~69%) of the analyzed zircon has a positive $\varepsilon_{Hf}(t)$ value (Fig. 6). These granitic rocks have higher $\varepsilon_{Hf}(t)$ and $\varepsilon_{Nd}(t)$ values than the Permian and Triassic granites. Similar to the Triassic felsic plutons, 66% ($\delta^{18}O > 7.0‰$) of the analyzed zircon grains have much higher $\delta^{18}O$ than mantle zircon (Valley, 2003; Fig. 6). A few inherited Archean zircon grains are also found in the Jurassic granites (Table S1 and Fig. 2).

The Cretaceous Liudong pluton consists of granodiorite and monzogranite. It still has weakly negative whole-rock $\varepsilon_{Nd}(t)$ value at -2.5. In contrast with the Permian tonalite, most zircon grains (~92%) in the rocks have positive $\varepsilon_{Hf}(t)$ with only minor (~8%) zircon having $\varepsilon_{Hf}(t) < 0$. However, the analyzed zircon has mantle-like $\delta^{18}O$ (5.4–6.5‰) value, which is almost identical to the range for the Permian tonalite ($\delta^{18}O = 5.4$–6.4‰, Fig. 6). The Hf−Nd isotopic variations shown by the granites in the SGZ have been widely observed in accretionary orogens (Collins et al., 2011), such as the Tasmanides in eastern Australia (Kemp et al., 2009).

4.2.2. The North Granite Zone (NGZ)

The Phanerozoic granitic rocks in the NGZ span an emplacement age between 267 and 112 Ma (Zhang et al., 2004; Wu et al., 2011; this

study). The Permian felsic plutons consist of plagiogranite and granodiorite, and have highly positive zircon $\varepsilon_{Hf}(t)$ between $+4.9$ and $+14.2$, with about half (44%) of the analyzed zircon having $\varepsilon_{Hf}(t) > +10$ (Table S2 and Fig. 7). They also show highly positive whole-rock $\varepsilon_{Nd}(t)$ value between $+3.3$ and $+3.8$ (Table 1). Zircon $\delta^{18}O$ values span a range of 4.2–6.1‰ with an average of 5.0‰, the lower limit of mantle-derived zircon (5.3 ± 0.3‰, Valley, 2003). About half (52%) of the analyzed zircon grains have $\delta^{18}O < 5.0‰$ (Fig. 7).

The Triassic granitic rocks include quartz diorite, monzogranite and syenogranite. They have positive whole-rock $\varepsilon_{Nd}(t)$ values between $+4.2$ and 2.2 (Table 1), and ~28% of the analyzed zircon grains show $\varepsilon_{Hf}(t) > +10$ (Fig. 7). Compared with the Permian felsic plutons, these rocks generally have lower $\varepsilon_{Hf}(t)$ and $\varepsilon_{Nd}(t)$ values, with a smaller proportion of the zircon having $\varepsilon_{Hf}(t) > +10$. The zircon spans a $\delta^{18}O$ range of 4.3–7.1‰ with an average of 5.4‰, and ~38% of the analyzed zircon grains have $\delta^{18}O < 5.0‰$ (Fig. 7). Compared to the Permian granitic plutons, fewer zircon grains in the Triassic granites have $\delta^{18}O$ values < 5.0‰.

The intensity of granitic magmatism in the NGZ peaked in the Jurassic. The Jurassic felsic intrusions mainly comprise granodiorite and monzogranite. They also have positive whole-rock $\varepsilon_{Nd}(t)$ values between $+3.3$ and 0, and ~15% of the analyzed zircon grains show $\varepsilon_{Hf}(t)$ values $> +10$ (Fig. 7). Compared with the Permian and Triassic felsic plutons, the proportion of the analyzed zircon with $\varepsilon_{Hf}(t) < +10$ is much higher (up to 85%). The zircon spans an $\delta^{18}O$ range of 3.8–7.5‰ with an average of 5.7‰. The proportion of the analyzed zircon with $\delta^{18}O < 5.0‰$ is low (14%).
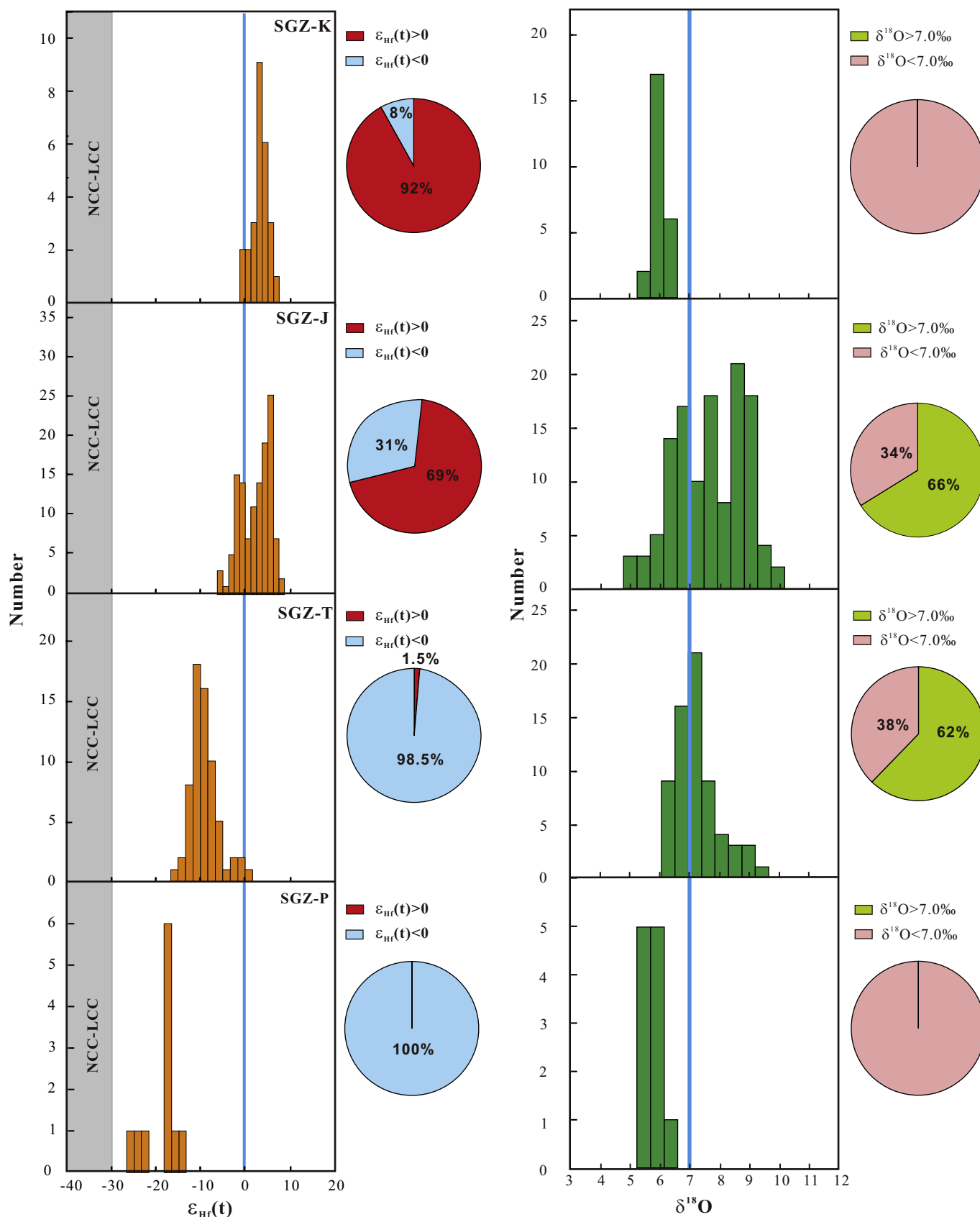
Fig. 6. Histograms of zircon Hf and O isotope compositions of Permian – Cretaceous granitic rocks in the South Granite Zone (SGZ). We suggest a sedimentary or metasedimentary origin for the zircon with $\delta^{18}O > 7‰$ and a recycled crust genesis for the zircon having $\varepsilon_{Hf}(t) < 0$.
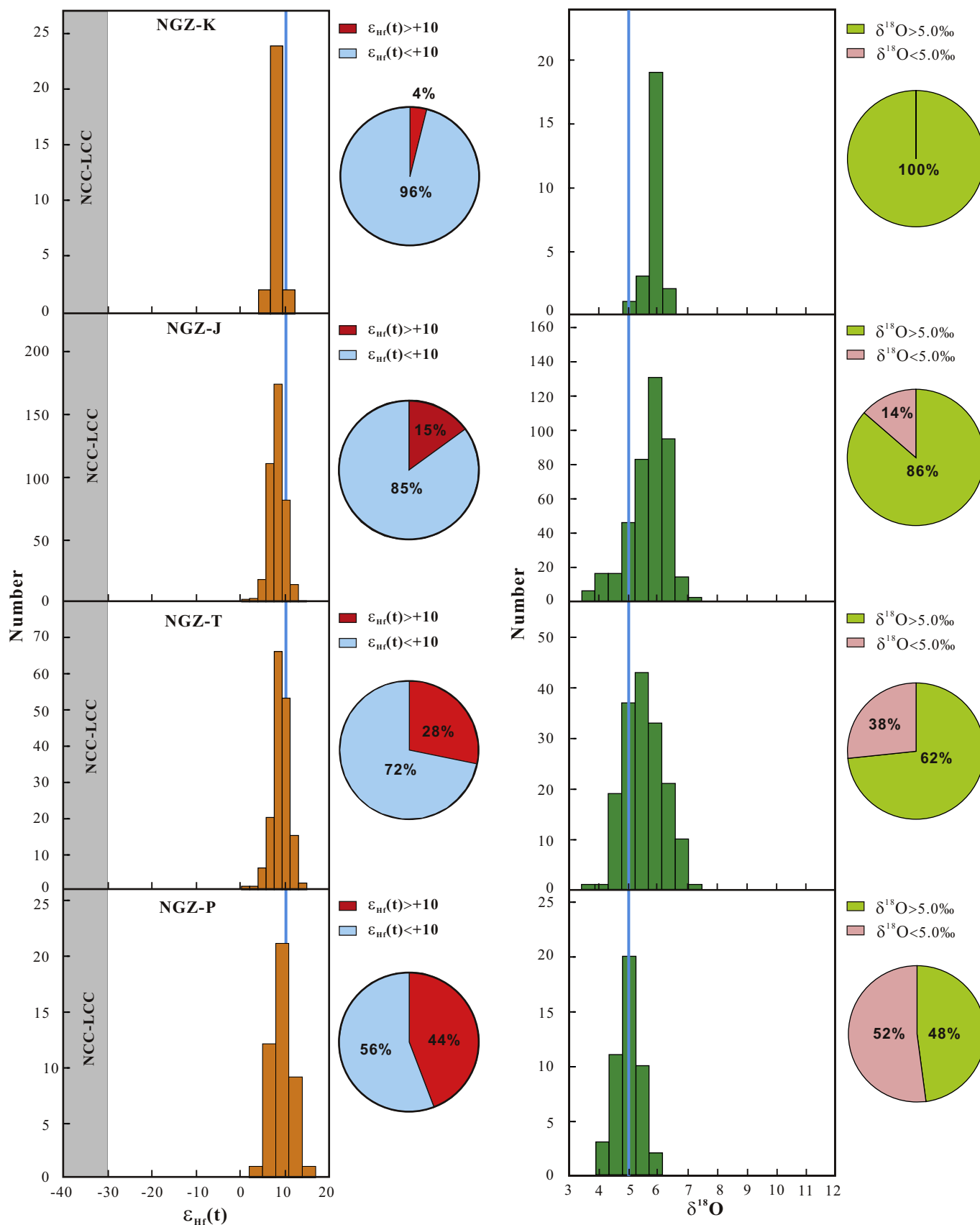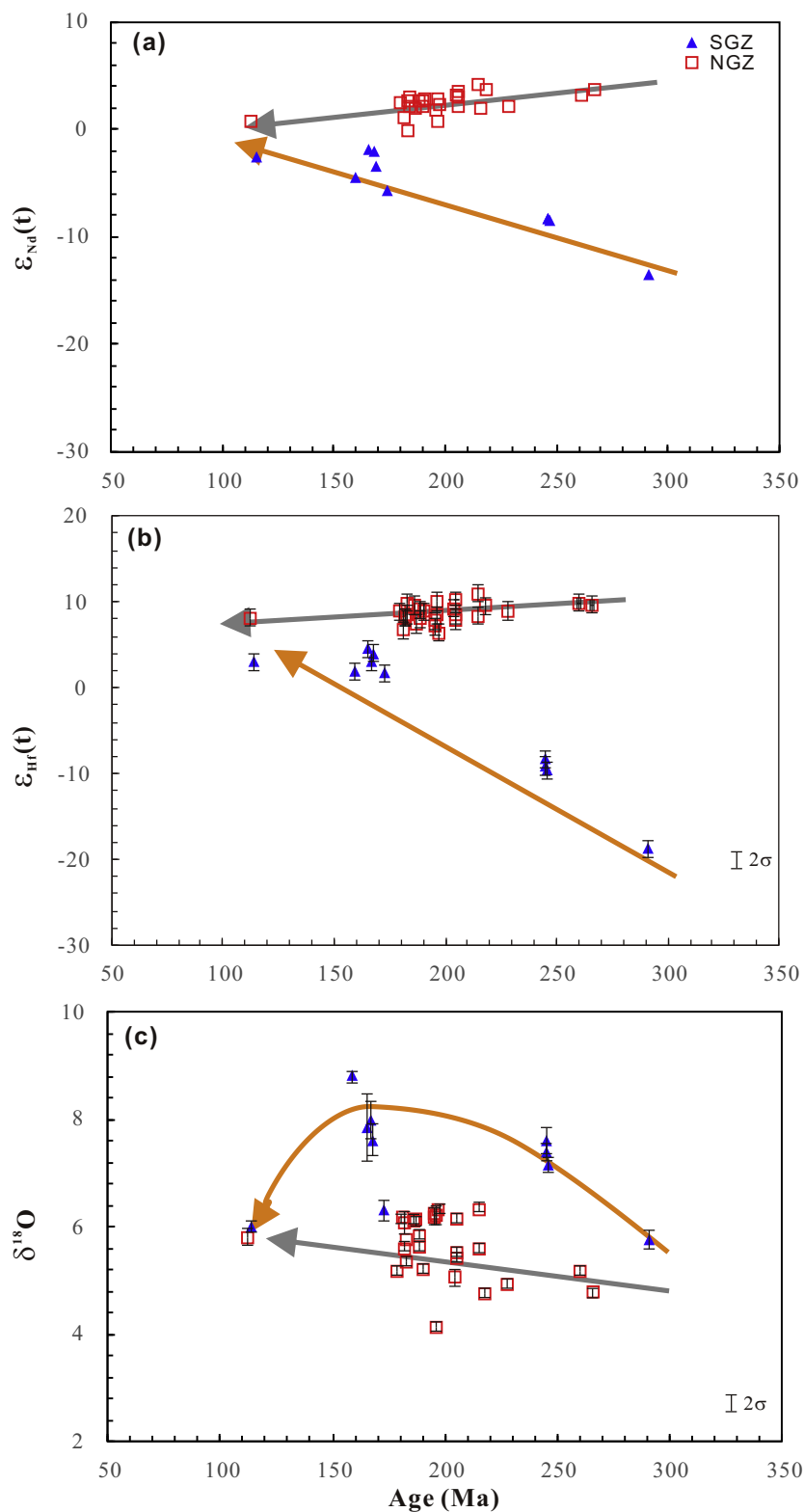
Fig. 7. Histograms of zircon Hf and O isotope compositions of Permian – Cretaceous granites in the North Granite Zone (NGZ). We suggest a hydrothermally altered oceanic crust origin for the zircon having $\varepsilon_{Hf}(t) > 10$ and $\delta^{18}O < 5\text{‰}$ (Wei et al., 2002).

Fig. 8. Variations of (a) whole-rock $\varepsilon_{Nd}(t)$, (b) zircon $\varepsilon_{Hf}(t)$ and (c) $\delta^{18}O$ against emplacement age (Ma) of Permian – Cretaceous granitic rocks in the Yanbian area. The whole-rock Nd isotope data are compiled from Huang et al. (2015) and references therein.

Granitic magmatism became less common during early Cretaceous and included the Xiaoxinancha pluton, which is composed of tonalite and monzogranite. They have positive whole-rock $\varepsilon_{Nd}(t)$ between $+0.9$ and $+1.7$ (Li et al., 2012a, 2012b). Although all zircon grains show positive $\varepsilon_{Hf}(t)$ values, only ~4% (one grain) has $\varepsilon_{Hf}(t) > +10$ (Fig. 7). The $\delta^{18}O$ range of zircon is between 5.2 and 6.2‰ with an average of

5.8‰. The observed decrease in both whole-rock $\varepsilon_{Nd}(t)$ and zircon $\varepsilon_{Hf}(t)$ from the Permian to Cretaceous NGZ granites is similar to isotopic trends noted in other collisional orogens, such as the Jurassic – Cretaceous Gangdese magmatic belt in Tibet plateau (Ji et al., 2009; Zhu et al., 2011) and the Ordovician – Silurian magmatism from the Tasmanides orogen in eastern Australia (Kemp et al., 2009).
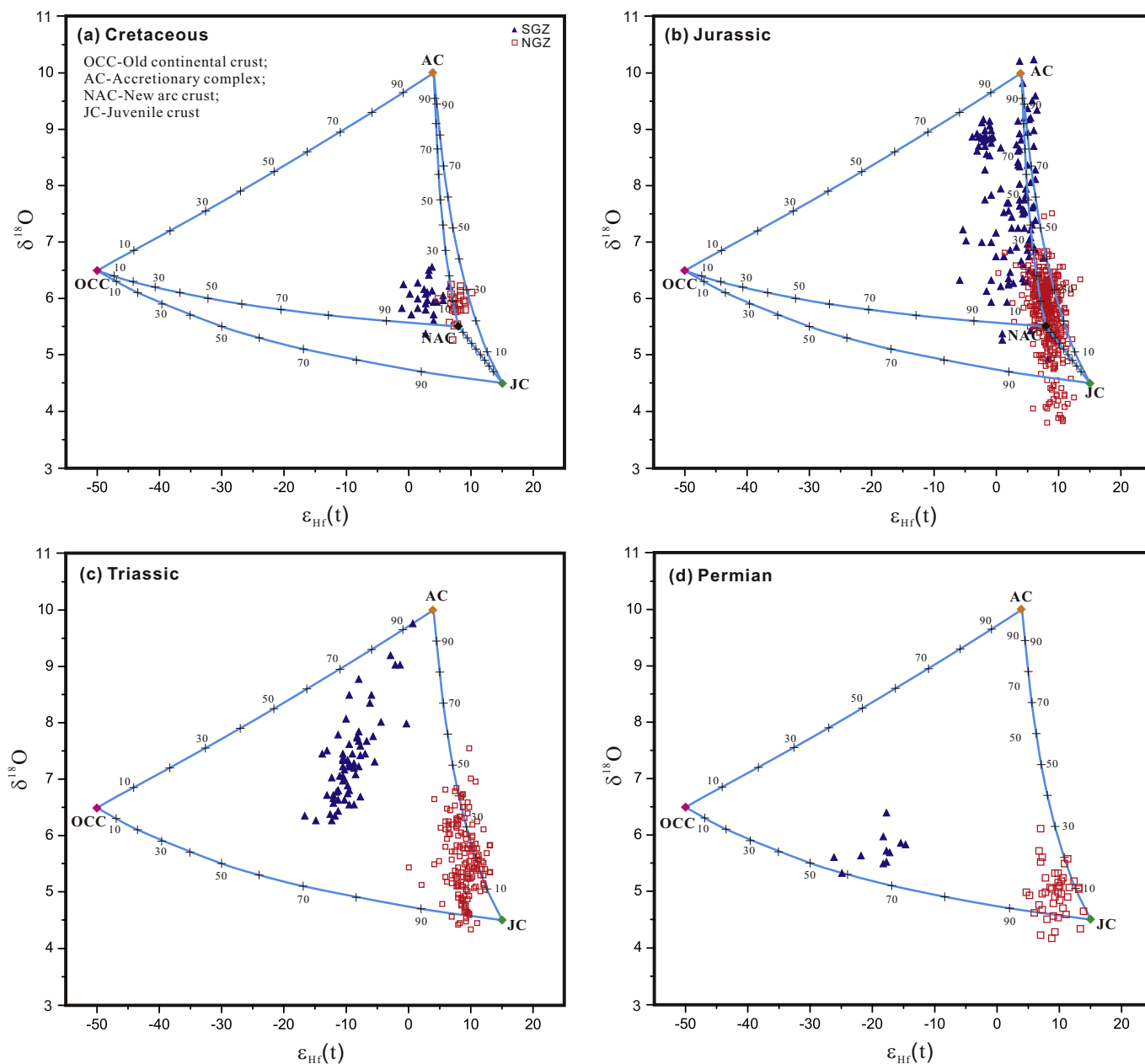
Fig. 9. Diagrams of zircon $\varepsilon_{Hf}(t)$ versus $\delta^{18}O$, showing the possible endmember components involved in the melting source for the Permian-Cretaceous granites from the Yanbian area, NE China. In accordance with the variation ranges of the Hf−O isotopes, we assume that the zircon from the (1) juvenile crust (JC) has $\varepsilon_{Hf}(t) = +15$, $\delta^{18}O = 4.5‰$ (Guo et al., 2016; Wei et al., 2002); (2) new arc crust (NAC) has $\varepsilon_{Hf}(t) = +8$, $\delta^{18}O = 5.5‰$ (Zhao et al., 2019); (3) accretionary complex (AC) has $\varepsilon_{Hf}(t) = +4$, $\delta^{18}O = 10‰$ (Wang et al., 2016); and (4) old continental crust (OCC) has $\varepsilon_{Hf}(t) = -50$, $\delta^{18}O = 6.5‰$ (Shen et al., 1992; Geng et al., 2012; this study). The ratio of Hf concentration among the crustal components is Hf_{JC}: Hf_{NAC}: Hf_{AC}:Hf_{OCC} = 1: 1: 2.5: 2.

To summarize the above observations, temporal trends in granite compositions in the SGZ are generally to higher whole-rock $\varepsilon_{Nd}(t)$ and zircon $\varepsilon_{Hf}(t)$ with decreasing crystallization age, whereas values for the NZG granitic rocks decrease (Fig. 8a and b). Zircon $\delta^{18}O$ in the SGZ granites increase from Permian to Jurassic and then decreases to Cretaceous, while values from the NGZ granitic rocks show a slight increase from Permian to Cretaceous (Fig. 8c). The isotopic difference between granites of the NGZ and SGZ is the greatest in Permian, but Nd-Hf-O isotopic compositions converge with decreasing formation age such that Cretaceous granitic rocks of the NGZ and SGZ are isotopically similar. Over the same period, the proportion of the zircon with $\varepsilon_{Hf}(t) < 0$ in the SGZ granites decreases significantly (Fig. 6), while the proportion of the zircon with $\varepsilon_{Hf}(t) > +10$ and $\delta^{18}O < 5.0‰$ in the NGZ granites also decreases (Fig. 7).

5. Discussion

The Phanerozoic granitic intrusions in the Yanbian area show distinct Nd-Hf-O isotopic variations between the SGZ and NGZ. The Permian to Cretaceous mafic magmatism, broadly contemporaneous with the granitic magma emplacement, is sporadically distributed in the Yanbian area, and the associated mafic microgranular enclaves within the granitic plutons are rare (Zhang et al., 2004; Wu et al., 2011; Guo et al., 2015, 2016; Ma et al., 2017). This indicates that mantle-derived magmas probably did not act as parental magmas for differentiation, nor were they an endmember component in a magma mixing relationship. The granitic rocks have strong I-type affinities (Fig. 3, Whalen et al., 1987), although we consider them to be melts of the crustal protoliths rather than being of direct mantle derivation. Their

A. Permian subduction of the Paleo-Asian Ocean and crustal growth
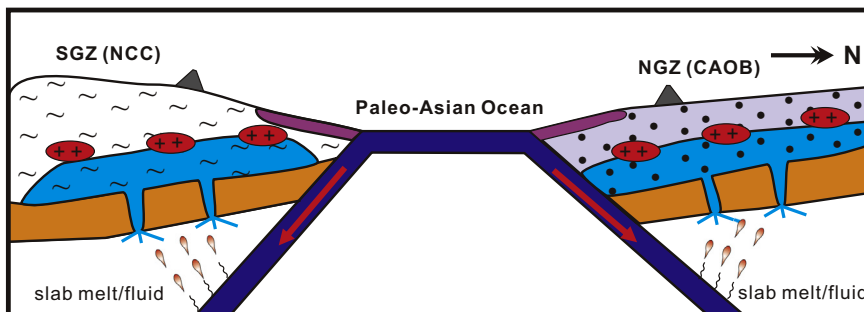
B. Triassic collision between the NCC and CAOB and crustal reworking
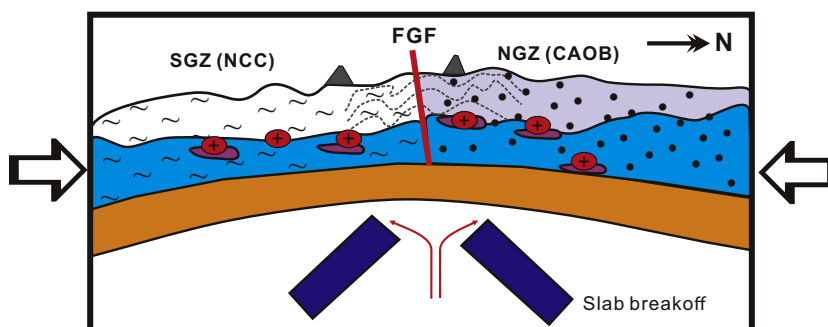
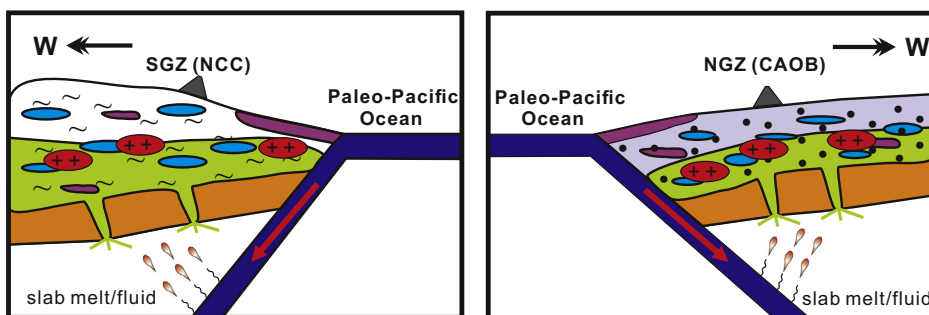C. Jurassic-Cretaceous subduction of the Paleo-Pacific Ocean and crustal replacement

Fig. 10. A cartoon showing crustal evolution of the Yanbian area, in which replacement of pre-existent crust by the new arc crust had occurred during subduction of both the paleo-Asian and paleo-Pacific Oceans.

Nd-Hf-O isotopic variations should thus reflect compositional variations in the crustal melting sources. In this regard, the differences in Nd-Hf-O isotopic compositions between the granitic rocks in the SGZ and NGZ can be interpreted in several ways, including: (1) lateral isotopic variations in the crustal source reflecting the presence of distinct tectonic units; (2) Vertical variation in crustal compositions resulting from episodic crustal growth and reworking events; and (3) Crustal heterogeneity as a result of replacement by new accreted crust. In the following section, we will assess the possible geodynamic processes that might have caused the observed systematic Hf-Nd-O isotopic variations in both zones. We then propose a new model to account for the crustal evolution along the Northeast Asian convergent plate margins. Finally, we investigate how relevant our new geodynamic model might be to other accretionary orogens.

5.1. Lateral geochemical variations between the SGZ and NGZ

Previous studies based on structural analysis, lithologic associations and Sr-Nd-Pb isotope mapping indicated that the Gudonghe-Fu'erhe Fault represented the boundary between the NCC and CAOB (Jia et al., 2004; Guo et al., 2010; Li et al., 2010a, 2010b). The NCC lower crust was principally formed during Archean to early Proterozoic and has developed moderately radiogenic Sr, highly non-radiogenic Nd and Hf and weakly radiogenic Pb compositions (e.g., Zhao et al., 2001; Zhou et al., 2002; Geng et al., 2012). Archean mafic granulite-facies rocks in the NCC have $\delta^{18}O$ between 6.0 and 8.0‰ (Shen et al., 1992), and consistent zircon O isotope values ($\delta^{18}O = 5.2–6.6$‰) are obtained for inherited Archean zircon in Permian Shiliping tonalite sample 13GF-46, from the SGZ (Table S2). These inherited zircon grains with Archean-early Proterozoic ages also show highly non-radiogenic Hf isotopic compositions (Tables S1 and 2). Both O and Hf isotope data
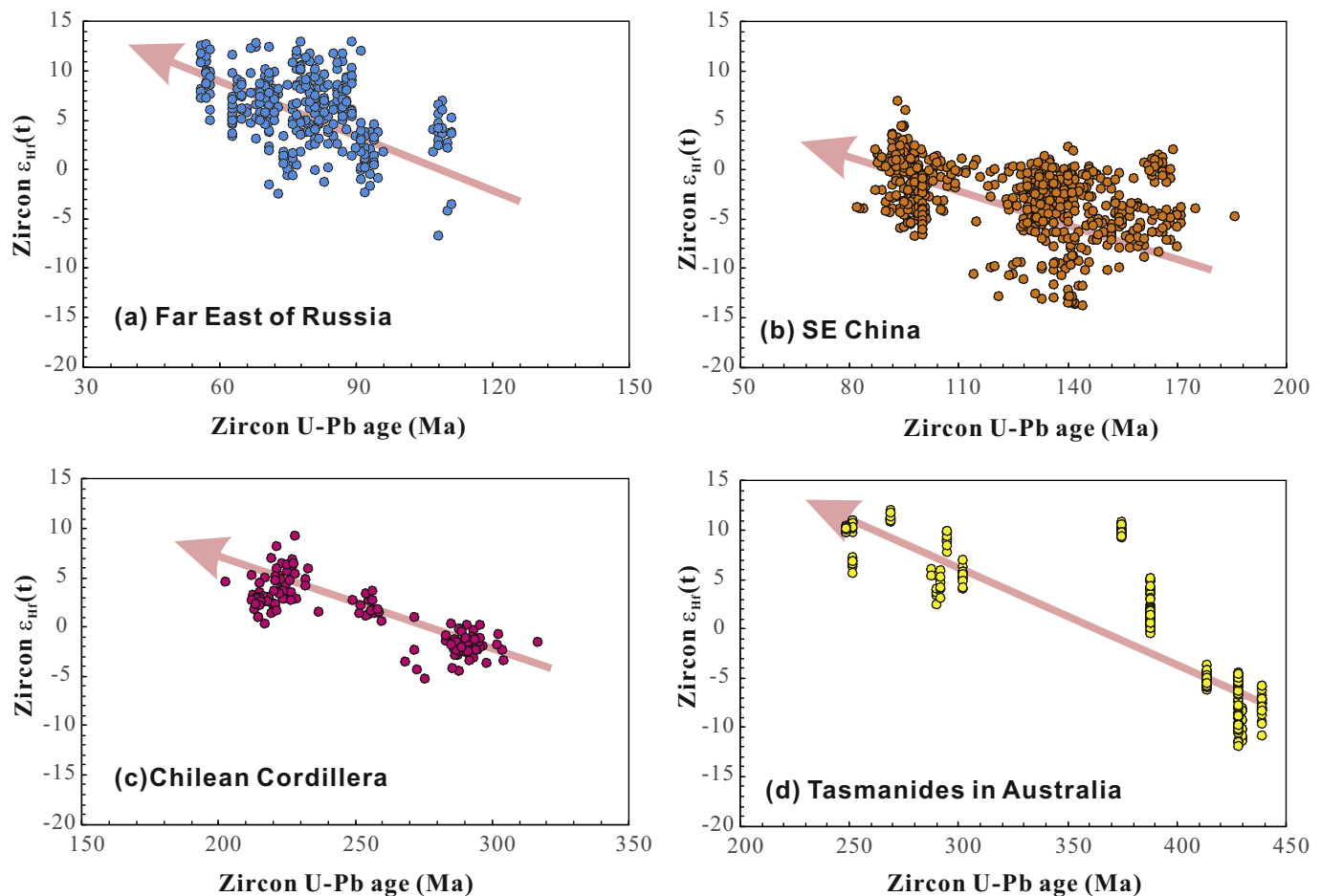
Fig. 11. Zircon U–Pb age versus $\varepsilon_{Hf}(t)$ for felsic igneous rocks in accretionary orogens. (a) Cretaceous to Tertiary granites in Far East of Russia (Jahn et al., 2015); (b) Jurassic to Cretaceous felsic volcanic rocks in SE China (Guo et al., 2012); (c) Carboniferous to Triassic granites in Chilean Cordillera (Hervé et al., 2014); (d) Silurian to Triassic granites in Australian Tasmanides (Kemp et al., 2009; Jeon et al., 2014).

($\delta^{18}O$ = 5.4–6.4‰; $\varepsilon_{Hf}(t) < < 0$) from the magmatic zircon also indicate an ancient mafic protolith component in the source of the tonalite. All these arguments indicate that the Permian Shiliping tonalitic intrusion was probably derived from a source consisting mainly of the ancient NCC crust.

By contrast, the CAOB consists of a series of subduction-accretionary complexes and Proterozoic – Paleozoic terranes such as the Erguna, Hinggan, Jiamusi and Khanka massifs (e.g., Xu et al., 2015; Liu et al., 2017a, 2017b). The crust is "juvenile" and has developed less radiogenic Sr and more radiogenic Nd, Hf and Pb isotopic compositions than the NCC, with some deep parts of crust even having lower $\delta^{18}O$ than mantle values (Jahn et al., 2000; Wu et al., 2000; Wei et al., 2002; Guo et al., 2010). These compositional features are reflected in Phanerozoic felsic magmas that generally have positive $\varepsilon_{Nd}(t)$ values and young T_{DM} (< 1.0 Ga) ages (e.g., Jahn et al., 2000; Wu et al., 2000; Guo et al., 2010). The Permian granodiorite and plagiogranite intrusions in the NGZ have highly radiogenic whole-rock Nd ($\varepsilon_{Nd}(t)$ = 3.3–3.8, Table S4) and zircon Hf isotopic compositions (half of the zircon has $\varepsilon_{Hf}(t) > +10$) as well as mantle-like $\delta^{18}O$ values (Table S2 and Fig. 9), indicating their derivation from a "juvenile" source typically of CAOB crust (Yang et al., 2006). Therefore, the isotopic difference of the Permian granitic rocks between the SGZ and NGZ can be simply attributed to the different tectonic units separated by the Fu'erhe-Gudonghe Fault. The crustal protoliths in the SGZ have been mainly inherited from the ancient NCC crust, whereas those in the NGZ have been derived from the CAOB "juvenile" crust.

5.2. Vertical variation in crustal compositions

Both the whole-rock $\varepsilon_{Nd}(t)$ and zircon $\varepsilon_{Hf}(t)$ increase significantly in the SGZ granitic rocks from Permian to Triassic, and this increase is coupled with an increase of zircon $\delta^{18}O$. About two thirds of the zircon grains have $\delta^{18}O > 7.0‰$, a signature of low-temperature alteration that is typically of surface or near-surface processes (Valley, 2003). This strongly implies the involvement of sedimentary or metasedimentary component in the melting source of the Triassic granites. As inferred from the variation trends in Figs. 7 and 9, the sedimentary component should have a positive $\varepsilon_{Hf}(t)$ value and is distinct from the Paleoproterozoic metasediments of NCC that have developed highly non-radiogenic Hf–Nd isotopic compositions (e.g., Geng et al., 2012; Liu et al., 2014). A likely candidate for such a component with positive $\varepsilon_{Hf}(t)$ and very high $\delta^{18}O$ is the material typically comprising a subduction-accretionary complex, where pelagic sediment, eroded arc igneous rock, altered oceanic crust and serpentine mixed together in response to the subduction of, in the present case, the paleo-Asian Ocean. Because the granitic magmas are generally melted at middle-lower crustal levels, possible mechanisms that might emplace this sedimentary component into the deep crust include: (1) crustal thickening in response to collision between the NCC and CAOB and subsequent burial of the accretionary complex to middle-lower crustal levels (Jeon et al., 2014), and (2) relamination of the accretionary complex at the base of the subarc crust (Hacker et al., 2011). Considering the ultimate closure of the paleo-Asian Ocean by the end of Permian (Zhou and Wilde, 2013; Wilde, 2015; Guo et al., 2016), we suggest that the accretionary

complex was likely emplaced in the deep crust during the collision between the NCC and CAOB.

Similarly, the involvement of a sedimentary component with high $\delta^{18}O$ and positive $\varepsilon_{Hf}(t)$ is also evident in the melting source of the Triassic granites from the NGZ, as reflected by the increase of zircon $\delta^{18}O$ and decrease of $\varepsilon_{Hf}(t)$ with decreasing age (Figs. 7 and 9). Correspondingly, the contribution of the "juvenile" component with low $\delta^{18}O$ (< 5.0‰) and highly radiogenic Hf ($\varepsilon_{Hf}(t) > +10$) is reduced when compared with the Permian granites. This isotopic change in the bulk melting source for the NGZ granitic magmas can be also ascribed to the collision between the NCC and CAOB.

The Hf−O isotopic variation trends continue from the Triassic to Jurassic granites in both zones. In the SGZ, the proportion of zircon with $\varepsilon_{Hf}(t) > 0$ increased significantly over this period (Fig. 6). However, this cannot again be attributed to the involvement of a subduction-accretionary complex component in the bulk melting source. For instance, some zircon grains have $\varepsilon_{Hf}(t)$ value around $+10$, but the proportion of zircon with $\delta^{18}O > 7.0‰$ shows little variation (Fig. 8). There must exist another source component that has similarly high $\delta^{18}O$ but much higher $\varepsilon_{Hf}(t)$ value (e.g., $\varepsilon_{Hf}(t) \sim +10$) than the subduction-accretionary complex. Considering the contemporaneous subduction of the paleo-Pacific Ocean and the resulting arc mafic magmatism (the zircon and whole-rock $\varepsilon_{Hf}(t) = +2 \sim +12$, zircon $\delta^{18}O = 5.6$–7.6‰; Yu et al., 2012; Guo et al., 2015; Zhao et al., 2019), it is reasonable to relate the Hf−O isotopic variations to the involvement of a newly accreted arc crust in the bulk crustal melting source (Fig. 9c). A few zircon grains have even higher $\delta^{18}O$ (> 9‰) and more radiogenic Hf ($\varepsilon_{Hf}(t) > +5$) than those of the Triassic granites (Table S2 and Fig. 9b). These likely reflect a contribution from subducted pelagic sediments, potentially as a result of relamination of accretionary complex components at the base of subarc crust (Hacker et al., 2011).

Systematic Hf−O isotopic variation trends are also observed from the Triassic to Jurassic granitic rocks in the NGZ. The proportion of zircon having $\varepsilon_{Hf}(t) > 10$ and $\delta^{18}O < 5.0‰$ continues to fall, whereas the percentage of zircon with $\varepsilon_{Hf}(t) < 10$ and $\delta^{18}O > 5.0‰$ increases. Possible mechanisms to interpret these isotopic variations include a heterogeneous lower-middle crust, and/or an addition of a newly accreted arc crust related to subduction of the paleo-Pacific Ocean.

In the case of a heterogeneous crust, a sedimentary source component would not only typically have developed more evolved isotopic compositions and higher $\delta^{18}O$ value, but it would have a higher water content than a metaigneous protolith and would melt at lower temperatures. Both the Triassic and Jurassic granitic rocks show similar incompatible trace element spidergrams (Fig. 4), suggesting comparable P-T conditions for crustal melting. Under similar P-T conditions, the earlier crustally derived melt should consume a higher proportion of any available sedimentary component and thus show more evolved isotopic compositions, i.e., lower whole-rock $\varepsilon_{Nd}(t)$ and zircon $\varepsilon_{Hf}(t)$ but higher $\delta^{18}O$ value. However, this is just contrasting with the geochemical observations between the Triassic and Jurassic granites in the NGZ. Therefore, melting of a heterogeneous lower-middle crust of the NGZ cannot interpret the geochemical variations from the Triassic to Jurassic granitic rocks (Fig. 10a and b). There must exist another component with less radiogenic Hf and Nd compositions and higher $\delta^{18}O$ than the Triassic granites. Again, the mafic arc-related intrusions in the Yanbian area, which contain moderately radiogenic Nd and Hf compositions and high $\delta^{18}O$ (Guo et al., 2015; Zhao et al., 2019), are likely candidate for a new arc crustal component that might have contributed to the bulk melting source for the Jurassic NGZ granites.

Granitic magmatism became uncommon during Cretaceous and in both zones the felsic magmas tend to be geochemically similar (Figs. 8 and 9). This compositional change indicates that the new arc crust became the predominant bulk melting source component for the Cretaceous granites across the Yanbian area.

5.3. Crustal replacement in the Yanbian area

From the discussion above, we suggest that the Nd-Hf-O isotopic variation trends observed in the Yanbian area indicate the existence of at least four crustal components in the melting source of granites: (1) a "juvenile" crust that has the highest $\varepsilon_{Nd}(t)$ and $\varepsilon_{Hf}(t)$ but the lowest $\delta^{18}O$, strongly resembling the CAOB crust; (2) a Precambrian crust with the lowest $\varepsilon_{Nd}(t)$ and $\varepsilon_{Hf}(t)$ and moderate $\delta^{18}O$, strongly resembling the ancient NCC crust; (3) a crustal component with moderate $\varepsilon_{Nd}(t)$ and $\varepsilon_{Hf}(t)$ but the highest $\delta^{18}O$, resembling the subduction-accretionary complex; and (4) a new arc crust with moderate $\varepsilon_{Nd}(t)$, $\varepsilon_{Hf}(t)$ and $\delta^{18}O$ (Fig. 9). The respective contribution of these crustal components has waned and waxed throughout the Phanerozoic history of granite generation in the Yanbian area.

As illustrated in Fig. 9, the contribution that the subduction-accretionary complex makes to the bulk crustal melting source of granites increases from Permian to Triassic, leading to an increase of zircon $\delta^{18}O$ in both zones. From the Permian to Triassic granites, zircon $\varepsilon_{Hf}(t)$ also increases in the SGZ, but it decreases slightly in the NGZ. Collision between the NCC and CAOB in early Triassic led to crustal thickening (Xiao et al., 2003; Wilde, 2015; Zhou and Wilde, 2013), during which the subduction-accretionary complex was buried to the lower-middle crustal depths. Similar zircon Hf−O isotopic variation trends have been documented in other orogenic belts, including the Tasmanides Orogen in eastern Australia (Kemp et al., 2009; Jeon et al., 2014), where the trends were attributed to back-arc closure and crustal shortening, accompanied by the formation of S-type granites.

The zircon $\delta^{18}O$ values of the Jurassic granitic rocks in the Yanbian area are slightly higher than those of the Triassic granites (Figs. 6 and 9), but both the whole-rock $\varepsilon_{Nd}(t)$ and zircon $\varepsilon_{Hf}(t)$ increase greatly, indicating an addition of a crustal component with radiogenic Nd and Hf to the bulk crustal melting source in the SGZ. According to Guo et al. (2015) and Zhao et al. (2019), the subduction-related mafic intrusions, which may represent the new arc crust, are characterized by moderately radiogenic Nd and Hf compositions and super-mantle $\delta^{18}O$ values in the Yanbian area. Invasion of these arc mafic intrusions could lead to replacement of the pre-existing crustal rocks, e.g., the subduction-accretionary complex and the Precambrian NCC crust in the SGZ. Cretaceous granodiorite shows similar Nd-Hf-O isotopic compositions to those arc mafic intrusions, reflecting a near complete dominance of the bulk crustal source of the granite by this new arc crust in response to subduction of the paleo-Pacific Ocean. This new arc crust was emplaced in the lower-middle crustal depths and dominated the bulk crustal melting source for the SGZ granites since Jurassic.

In the NGZ, crustal replacement must also be invoked to explain the Nd-Hf-O isotopic variation trends of the Permian to Cretaceous granitic rocks. Because the CAOB crust was "juvenile" in terms of Nd and Hf isotopes, e.g., the Permian subduction-related mafic intrusions, which may represent the CAOB crust, have developed more radiogenic Nd and Hf compositions (the whole-rock $\varepsilon_{Nd}(t)$ and $\varepsilon_{Hf}(t)$ can be as high as 6.8 and 14.6, respectively, Guo et al., 2016) than the Jurassic arc mafic rocks (Zhao et al., 2019). Addition of the new arc crust represented by the Jurassic arc-related mafic intrusions would lead to decreases of both the whole-rock $\varepsilon_{Nd}(t)$ and zircon $\varepsilon_{Hf}(t)$ values. The scarcity of zircon with $\delta^{18}O > 7.0‰$ (< 1%, Table S2) in these granitic rocks indicates a minor contribution of sedimentary or metasedimentary protoliths to their bulk melting sources. We therefore attribute the lowering of zircon $\varepsilon_{Hf}(t)$ and the slight increase of $\delta^{18}O$ to replacement of the pre-existing "juvenile" crustal rocks by the new arc crust. Emplacement of the arc mafic magmas resulted in the progressive consumption of the "juvenile" crustal component. Similar Nd−Hf isotopic variations can be observed in the Gangdese batholith from the Tibet Plateau (Ji et al., 2009; Zhu et al., 2011), where the Jurassic to Cretaceous granitic rocks show decreasing zircon $\varepsilon_{Hf}(t)$ in response to subduction of the Tethyan Ocean.

Although underplating of mantle-derived mafic magmas and relamination of felsic components may also lead to crustal accretion and

reworking in convergent plate margins, these processes are unlikely to have had a dominant control over the compositional evolution of extensive Phanerozoic granitic magmatism in the Yanbian area. On one hand, during underplating and lower crustal invasion of mafic arc magmas, the composition of crust-derived melt depends strongly on the composition of the crust, in particular the proportion of hydrous minerals, the temperature and water content of the underplating magma (Petford and Gallagher, 2001; Annen and Sparks, 2002). Crustal anatexis will be limited when a wet and cool basalt (e.g., hydrous arc magma) invades anhydrous infertile crust (e.g., Precambrian crust or amphibolite and mafic granulite). It is thus unlikely that underplating of hydrous arc magmas such as the mafic intrusions (hornblende gabbro and diorite) in the Yanbian area (Yu et al., 2012; Guo et al., 2015; Zhao et al., 2019) would result in the observed widespread occurrence of I-type granites and their eruptive counterparts, which require extensive melting of metaigneous protoliths. On the other hand, relamination of felsic material (e.g., subducted sediment) beneath the subarc crust would form a more felsic hybrid crust that is much easier to melt. Since the relaminated materials generally have non-radiogenic Nd and Hf compositions and high $\delta^{18}O$, addition of this felsic component would lower the Nd and Hf isotope ratios and elevate $\delta^{18}O$ of the bulk melting source. This might, to some degree, have interpreted the observed isotopic variation trends in the NGZ granites, which shows decreases of both $\varepsilon_{Nd}(t)$ and $\varepsilon_{Hf}(t)$ and a slight increase of $\delta^{18}O$ from Permian to Cretaceous (Fig. 8). However, the Cretaceous tonalite in the NGZ has among the highest Mg#, Sr/Y and $(La/Yb)_N$ but the lowest Rb/Sr and Eu/Eu* ratios (Table S4), indicating a more mafic crustal protolith and a greater melting pressure with little or no residual plagioclase in the source (Patiño Douce and Beard, 1995; Guo et al., 2012; Ma et al., 2015). Even if it had occurred during Permian to Cretaceous, this inconsistency between the Nd−Hf isotope data and chemical compositions suggests a minor role of relamination during the crustal evolution of the NGZ. In the case of SGZ, relamination of a felsic component appears negligible since the isotopic variation trends of Triassic to Cretaceous granites indicate a predominant contribution from a "juvenile" component.

Based on the discussion above, we propose a new geodynamic model for crustal evolution in the Yanbian area, which emphasizes that the crustal sources for the granitic rocks in both zones have been largely or almost completely replaced by the new arc crust in response to subduction of the paleo-Pacific Ocean, as envisaged in Fig. 10. During the Permian (Fig. 10A), double-sided subduction of the paleo-Asian Ocean led to crustal accretion in both the SGZ and NGZ. In the course of subduction, the overlying lithospheric mantle and lower crust were eroded and even removed by the corner flow from the convective asthenosphere and the subducting paleo-Asian oceanic slab (e.g., Vogt et al., 2012; von Huene et al., 2004). In the SGZ, the Precambrian NCC crust was eroded and modified by an addition of the "juvenile" crust. Remelting of the hybrid crust with predominant Precambrian NCC crustal protoliths formed the Permian tonalite. Accretion of the "juvenile" crust into the subduction-related accretionary complex formed another hybrid crustal source for the Permian granites in the NGZ. In the Triassic (Fig. 10B), collision between the NCC and CAOB led to crustal shortening and thickening, and anatexis of the thickened crust composed of the subduction-accretionary complex and the pre-existing crustal protoliths in both zones formed the granitic magmas. Since the early Jurassic (Fig. 10C and D), subduction of the paleo-Pacific Ocean has led to extensive arc magmatism. The pre-existing crustal components in both zones were largely eroded and destructed by the subducting paleo-Pacific slab and mechanically removed by the corner flow of asthenosphere (e.g., Vogt et al., 2012; von Huene et al., 2004). Subsequent invasion of the Jurassic arc-related mafic intrusions further diluted, destroyed and replaced the pre-existing crustal rocks. The degree of replacement reached at its maximum in early Cretaceous when the composition of bulk crustal melting sources became virtually indistinguishable. In the SGZ, the NCC Precambrian crust had been almost completely replaced by both the "juvenile" and new arc crust respectively in association with the Paleozoic and Mesozoic subduction of the paleo-Asian and paleo-Pacific Oceans.

5.4. Crustal replacement in accretionary orogens

In a global scale, Collins et al. (2011) divided orogens into two types: internal and external orogen. They further demonstrated that zircon ε_{Hf} values of granites in external orogens show a negative correlation with the emplacement age. The external orogen are comparable with the classic accretionary orogens, such as those in the circum-Pacific Ocean. Here, we compile data from granitic rocks and their eruptive counterparts in Far East of Russia (Jahn et al., 2015), SE China (Guo et al., 2012), the Chilean Cordillera (Hervé et al., 2014) and the Tasmanides in eastern Australia (Kemp et al., 2009; Jeon et al., 2014), to investigate the possible role of crustal replacement in these orogens.

In the case of Far East of Russia, which lies adjacent to the Yanbian area, the majority of the Cretaceous – Paleocene granitic rocks have negative $\varepsilon_{Nd}(t)$ (Jahn et al., 2015), although some zircon grains show $\varepsilon_{Hf}(t)$ as high as +15 (Fig. 11a). Eastward migration of subduction zone was likely caused by retreat of the trench and rollback of the subducting paleo-Pacific slab. Emplacement of mafic arc magmas and of possible back-arc basalts changed the bulk crustal source towards more "juvenile" compositions. Therefore, subduction-induced crustal replacement, as envisaged for the Yanbian area, can also account for the Hf−Nd isotopic variations in this region.

In SE China, the Jurassic – Cretaceous felsic volcanic rocks also show a broad negative correlation between zircon U−Pb age and $\varepsilon_{Hf}(t)$ (Fig. 11b). The subduction-related mafic intrusions in this area also have similarly positive $\varepsilon_{Hf}(t)$ (e.g., Chen et al., 2013; Zhang et al., 2019), suggesting an important contribution from arc magmas to the bulk crustal source for the felsic melts. Through a process similar to emplacement of new arc crust proposed for the Yanbian area, the underplated mafic intrusions modified and replaced the pre-existent Proterozoic crust of SE China.

In the Chilean Cordillera, the zircon $\varepsilon_{Hf}(t)$ of granites increased between 300 and 215 Ma with a decrease of zircon $\delta^{18}O$ below normal mantle at ca. 230 Ma and then an increase of $\delta^{18}O$ to 215 Ma (Fig. 11c, Hervé et al., 2014). Such Hf−O isotope variations reflect the transition from a subduction-related setting into a rift. The pre-existing crust was extensively modified and replaced by rift-related "juvenile" crust.

In the Tasmanides orogen, zircon $\varepsilon_{Hf}(t)$ increased significantly to MORB-like values from 430 to 250 Ma (Fig. 11d), followed by an increase of whole-rock $\varepsilon_{Nd}(t)$ and a decrease of $\delta^{18}O$ to depleted mantle value (Kemp et al., 2009). Such isotopic variation trends are consistent with the retreat of the trench and the rollback of the subducting slab (Vogt et al., 2012), during which partial melting of the upwelling asthenospheric mantle formed the mafic magma with depleted mantle-type Hf-Nd-O isotopic compositions. Underplating of the basaltic melt modified the crustal composition, which can be also interpreted as replacement by "juvenile" crustal component in an extensional accretionary orogen (Kemp et al., 2009).

6. Concluding remarks

Two contrasting Nd-Hf-O isotopic variation trends have been identified in the Permian - Cretaceous granitic rocks from two adjacent zones within the Yanbian area, NE China and indicate the subduction-induced crustal replacement in both granite zones. Emplacement of the new arc crust has led to destruction, erosion, dilution and replacement of the pre-existent crust, especially in the SGZ, where the Precambrian crust of NCC had been almost entirely replaced by the Paleozoic "juvenile" crust and Mesozoic new arc crust respectively related to subduction of the paleo-Asian and paleo-Pacific Oceans. The two types of Nd-Hf-O isotopic variation trends observed in the Yanbian area can be widely observed in other accretionary orogens, suggesting that crustal

replacement is an important process promoting crustal growth and re-working in convergent plate margins.

Supplementary data to this article can be found online at https://doi.org/10.1016/j.chemgeo.2019.07.013.

Acknowledgements

References

Anderson, T., 2002. Correction of common lead in U-Pb analyses that do not report [204]Pb. Chem. Geol. 192, 59–79.

Annen, C., Sparks, R.S.J., 2002. Effects of repetitive emplacement of basaltic intrusions on thermal evolution and melt generation in the crust. Earth Planet. Sci. Lett. 203, 937–955.

Black, L.P., Kamo, S.L., Allen, C.M., Aleinikoff, J.N., Davis, D.W., Korsch, R.J., Foudoulis, C., 2003. TEMORA 1: a new zircon standard for Phanerozoic U–Pb geochronology. Chem. Geol. 200, 155–170.

Bouvier, A., Vervoort, J.D., Patchett, P.J., 2008. The Lu–Hf and Sm–Nd isotopic composition of CHUR: constraints from unequilibrated chondrites and implications for the bulk composition of terrestrial planets. Earth Planet. Sci. Lett. 273, 48–57.

Chauvel, C., Garçon, M., Bureau, S., Besnault, A., Jahn, B.M., Ding, Z.L., 2014. Constraints from loess on the Hf–Nd isotopic composition of the upper continental crust. Earth Planet. Sci. Lett. 388, 48–58.

Chen, J.Y., Yang, J.H., Zhang, J.H., Sun, J.F., Wilde, S.A., 2013. Petrogenesis of the Cretaceous Zhangzhou batholith in southeastern China: Zircon U–Pb age and Sr–Nd–Hf–O isotopic evidence. Lithos 162, 140–156.

Collins, W.J., Belousova, E.A., Kemp, A.S.I., Murphy, J.B., 2011. Two contrasting Phanerozoic orogenic systems revealed by hafnium isotope data. Nat. Geosci. 4, 333–337.

DePaolo, D.J., 1981. Neodymium isotopes in the Colorado Front Range and crust-mantle evolution in the Proterozoic. Nature 291, 193–196.

Fisher, C.M., Hanchar, J.M., Samson, S.D., Dhuime, B., Blichert-Toft, J., Vervoort, J.D., Lam, R., 2011. Synthetic zircon doped with hafnium and rare earth elements: a reference material for in situ hafnium isotope analysis. Chem. Geol. 286, 32–47.

Gao, S., Rudnick, R.L., Yuan, H.L., Liu, X.M., Liu, Y.S., Xu, W.L., Ling, W.L., Ayers, J., Wang, X.C., Wang, Q.H., 2004. Recycling lower continental crust in the North China craton. Nature 432, 892–897.

Geng, Y.S., Du, L.L., Ren, L.D., 2012. Growth and reworking of the early Precambrian continental crust in the North China Craton: Constraints from zircon Hf isotopes. Gondwana Res. 21, 517–529.

Guo, F., Nakamura, E., Fan, W.M., Kobayashi, K., Li, C.W., 2007. Generation of Palaeocene adakitic andesites by magma mixing; Yanji Area, NE China. J. Petrol. 48, 661–692.

Guo, F., Fan, W.M., Gao, X.F., Li, C.W., Miao, L.C., Zhao, L., Li, H.X., 2010. Sr-Nd-Pb isotope mapping of Mesozoic igneous rocks in NE China: constraints on tectonic framework and Phanerozoic crustal growth. Lithos 120, 563–578.

Guo, F., Fan, W.M., Li, C.W., Zhao, L., Li, H.X., Yang, J.H., 2012. Multi-stage crust–mantle interaction in SE China: Temporal, thermal and compositional constraints from the Mesozoic felsic volcanic rocks in eastern Guangdong-Fujian provinces. Lithos 150, 62–84.

Guo, F., Fan, W.M., Li, C.W., Wang, C.Y., Li, H.X., Zhao, L., Li, J.Y., 2014. Hf–Nd–O isotopic evidence for melting of recycled sediments beneath the Sulu Orogen, North China. Chem. Geol. 381, 243–258.

Guo, F., Li, H.X., Fan, W.M., Li, J.Y., Zhao, L., Huang, M.W., Xu, W.L., 2015. Early Jurassic subduction of the Paleo-Pacific Ocean in NE China: petrologic and geochemical evidence from the Tumen mafic intrusive complex. Lithos 224-225, 46–60.

Guo, F., Li, H.X., Fan, W.M., Li, J.Y., Zhao, L., Huang, M.W., 2016. Variable sediment flux in generation of Permian subduction-related mafic intrusions from the Yanbian region, NE China. Lithos 261, 195–215.

Hacker, B.R., Kelemen, P.B., Behn, M.D., 2011. Differentiation of the continental crust by relamination. Earth Planet. Sci. Lett. 307, 501–516.

Hawkesworth, C.J., Kemp, A.I.S., 2006. The differentiation and rates of generation of the continental crust. Chem. Geol. 226, 134–143.

Hervé, F., Fanning, C.M., Calderón, M., Mpodozis, C., 2014. Early Permian to Late Triassic batholiths of the Chilean Frontal Cordillera (28°–31°S): SHRIMP U–Pb zircon ages and Lu–Hf and O isotope systematics. Lithos 184–187, 436–446.

Horstwood, M.S.A., Košler, J., Gehrels, G., Jackson, S.E., McLean, N.M., Paton, C.,

Pearson, N.J., Sircombe, K., Sylvester, P., Vermeesch, P., Bowring, J.F., Condon, D.J., Schoene, B., 2016. Community-derived standards for LA-ICP-MS U-(Th-)Pb geochronology – uncertainty propagation, age interpretation and data reporting. Geostand. Geoanal. Res. 40, 311–332.

Huang, M.W., Guo, F., Zhao, L., Li, Y.Y., 2015. Nd isotope constraint on crustal replacement induced by subduction of Paleo-Pacific Plate in the Yanbian area, NE China. Geotecton. Metallog. 39, 446–459 (in Chinese with English abstract).

von Huene, R., Ranero, C., Vannucchi, P., 2004. Generic model of subduction erosion. Geology 32, 913–916.

Jahn, B.M., Wu, F.Y., Chen, B., 2000. Massive granitoid generation in Central Asia: Nd isotope evidence and implication for continental growth in the Phanerozoic. Episodes 23, 82–92.

Jahn, B.M., Valui, G., Kruk, N., Gonevchuk, V., Usuki, M., Wu, T.J., 2015. Emplacement ages, geochemical and Sr–Nd–Hf isotopic characterization of Mesozoic to early Cenozoic granitoids of the Sikhote-Alin Orogenic Belt, Russian Far East: Crustal growth and regional tectonic evolution. J. Asian Earth Sci. 111, 872–918.

Jeon, H., Williams, I.S., Bennett, V.C., 2014. Uncoupled O and Hf isotopic systems in zircon from the contrasting granite suites of the New England Orogen, eastern Australia: Implications for studies of Phanerozoic magma genesis. Geochim. Cosmochim. Acta 146, 132–149.

Ji, W.Q., Wu, F.Y., Chung, S.L., Li, J.X., Liu, C.Z., 2009. Zircon U–Pb geochronology and Hf isotopic constraints on petrogenesis of the Gangdese batholith, southern Tibet. Chem. Geol. 262, 229–245.

Jia, D.C., Hu, R.Z., Lu, Y., Qiu, X.L., 2004. Collision belt between the Khanka block and the North China block in the Yanbian Region, Northeast China. J. Asian Earth Sci. 23, 211–219.

Kay, R.W., Kay, S.M., 1993. Delamination and delamination magmatism. Tectonophysics 219, 177–189.

Kemp, A.I.S., Hawkesworth, C.J., Paterson, B.A., Kinny, P.D., 2006. Episodic growth of the Gondwana supercontinent from hafnium and oxygen isotopes in zircon. Nature 439, 580–583.

Kemp, A.I.S., Hawkesworth, C.J., Collins, W.J., Gray, C. M., Blevin, P.L., EIMF, 2009. Isotopic evidence for rapid continental growth in an extensional accretionary orogen: the Tasmanides, eastern Australia. Earth Planet. Sci. Lett. 284, 455–466.

Košler, J., Sláma, J., Belousova, E., Corfu, F., Gehrels, G.E., Gerdes, A., Horstwood, M.S.A., Sircombe, K.N., Sylvester, P.J., Tiepolo, M., Whitehouse, M.J., Woodhead, J.D., 2013. U-Pb detrital zircon analysis - results of an inter-laboratory comparison. Geostand. Geoanal. Res. 37, 243–259.

Li, C.W., Guo, F., Fan, W., Gao, X., 2007. Ar–Ar geochronology of late Mesozoic volcanic rocks from the Yanji area, NE China and tectonic implications. Sci. China Ser. D Earth Sci. 50, 505–518.

Li, X.H., Liu, Y., Li, Q.L., Guo, C.H., Chamberlain, K.R., 2009. Precise determination of Phanerozoic zircon Pb/Pb age by multicollector SIMS without external standardization. Geochem. Geophys. Geosyst. 10, 1–21.

Li, C.W., Guo, F., Zhao, L., Li, H.X., 2010a. Geochemical constraints on petrogenesis of Late Mesozoic intermediate-felsic volcanic rocks from the southeastern Jilin Province, NE China. Acta Petrol. Sin. 26, 1074–1088 (in Chinese with English abstract).

Li, X.H., Li, W.X., Li, Q.L., Wang, X.C., Liu, Y., Yang, Y.H., 2010b. Petrogenesis and tectonic significance of the ~850Ma Gangbian alkaline complex in South China: evidence from in situ U-Pb dating, Hf-O isotopes and whole-rock geochemistry. Lithos 114, 1–15.

Li, H.X., Guo, F., Li, C.W., Zhao, L., 2012a. Petrogenesis of early cretaceous tonalites from the Xiaoxinancha Au-Cu deposit. Geochimica 41, 497–514 (in Chinese with English abstract).

Li, C.Y., Zhang, H., Wang, F.Y., Liu, J.Q., Sun, Y.L., Hao, X.L., Li, Y.F., Sun, W.D., 2012b. The formation of the Dabaoshan porphyry molybdenum deposit induced by slab rollback. Lithos 150, 101–110.

Liang, X.R., Wei, G.J., Li, X.H., Liu, Y., 2003. Precise measurement of [143]Nd/[144]Nd and Sm/Nd ratios using multiple-collectors inductively coupled plasma-mass spectrometer (MC-ICPMS). Geochimica 32, 91–96 (in Chinese with English abstract).

Liu, Y.S., Hu, Z.C., Gao, S., Gunther, D., Xu, J., Gao, C.G., Chen, H.H., 2008. In situ analysis of major and trace elements of anhydrous minerals by LA–ICP-MS without applying an internal standard. Chem. Geol. 257, 34–43.

Liu, C.H., Zhao, G.C., Liu, F.L., 2014. Detrital zircon U–Pb, Hf isotopes, detrital rutile and whole-rock geochemistry of the Huade Group on the northern margin of the North China Craton: implications on the breakup of the Columbia supercontinent. Precambrian Res. 254, 290–305.

Liu, Y.J., Li, W.M., Feng, Z.Q., Wen, Q.G., Neubauer, F., Liang, C.Y., 2017a. A review of the Paleozoic tectonics in the eastern part of Central Asian Orogenic Belt. Gondwana Res. 43, 123–148.

Liu, K., Zhang, J.J., Wilde, S.A., Liu, S.R., Guo, F., Kasatkin, S.A., Golozoubov, V.V., Ge, M.H., Wang, M., Wang, J.M., 2017b. U-Pb dating and Lu-Hf isotopes of detrital zircons from the southern Sikhote-Alin Orogenic Belt, Russian Far East: tectonic implications for the early Cretaceous evolution of the northwest Pacific margin. Tectonics 36, 2555–2598.

Ludwig, K.R., 2003. ISOPLOT 3.0: A Geochronological Toolkit for Microsoft Excel. Berkeley Geochronology Center Special Publications, pp. 4.

Ma, Q., Zheng, J.P., Xu, Y.G., Griffin, W.L., Zhang, R.S., 2015. Are continental "adakites" derived from thickened or foundered lower crust? Earth Planet. Sci. Lett. 419, 125–133.

Ma, X.H., Zhu, W.P., Zhou, Z.H., Qiao, S.L., 2017. Transformation from Paleo-Asian Ocean closure to Paleo-Pacific subduction: new constraints from granitoids in the eastern Jilin–Heilongjiang Belt, NE China. J. Asian Earth Sci. 144, 261–286.

Maruyama, S., Liou, J.G., Seno, T., 1989. Mesozoic and Cenozoic evolution of Asia. In: Ben-Avraham, Z. (Ed.), The Evolution of the Pacific Ocean Margins. Oxford

Monography of Geology and Geophysics, vol. 8. pp. 75–99.

Patiño Douce, A.E., Beard, J.S., 1995. Dehydration-melting of biotite gneiss and quartz amphibolite from 3 to 15 kbar. J. Petrol. 36, 707–738.

Petford, N., Gallagher, K., 2001. Partial melting of mafic (amphibolitic) lower crust by periodic influx of basaltic magma. Earth Planet. Sci. Lett. 193, 483–499.

Qi, L., Hu, J., Conard, G.D., 2000. Determination of trace elements in granites by inductively coupled plasma mass spectrometry. Talanta 51, 507–513.

Rudnick, R.L., Gao, S., 2003. Composition of the Continental Crust. In: Holland, H., Turekian, K. (Eds.), Treatise on Geochemistry. vol. 3. Elsevier, Amsterdam, pp. 1–64.

Sengör, A.M.C., Natal'in, B.A., Burtman, V.S., 1993. Evolution of the Altaid tectonic collage and Paleozoic crustal growth in Eurasia. Nature 364, 299–307.

Shen, Q.H., Xu, H.F., Zhang, Z.Q., 1992. Early Precambrian Granulites in China. Geological Press, Beijing (1-237 pp (in Chinese)).

Spencer, C.J., Kirkland, C.L., Taylor, R.J.M., 2016. Strategies towards statistically robust interpretations of in situ U–Pb zircon geochronology. Geosci. Front. 7, 581–589.

Sun, S.S., McDonough, W.F., 1989. Chemical and isotopic systematics of oceanic basalts: Implications for mantle composition and processes. In: Saunders, A.D., Norry, M.J. (Eds.), Magmatism in the Ocean Basins. Geol. Soc. London Spec. Pub, vol. 42. pp. 313–345.

Tanaka, T., Togashi, S., Kamioka, H., Amakawa, H., Kagami, H., Hamamoto, T., Yuhara, M., Orihashi, Y., Yoneda, S., Shimizu, H., Takahashi, K., Yanagi, T., Nakano, T., Fujimaki, H., Shinjo, R., Asahara, Y., Tanimizu, M., Dragusanu, C., 2000. JNdi-1: a neodymium isotopic reference in consistency with LaJolla neodymium. Chem. Geol. 168, 179–181.

Tang, K.D., 1990. Tectonic development of Paleozoic fold belts at the north margin of the Sino-Korean craton. Tectonics 9, 249–260.

Taylor, S.R., McLennan, S.M., 1985. The Continental Crust: Its Composition and Evolution. Blackwell Press, Oxford (1-312 pp).

Valley, J.W., 2003. Oxygen isotopes in zircon. Rev. Mineral. Geochem. 53, 343–385.

Vervoort, J.D., Kemp, A.I.S., 2016. Clarifying the zircon Hf isotope record of crust–mantle evolution. Chem. Geol. 425, 65–75.

Vogt, K., Gerya, T.V., Castro, A., 2012. Crustal growth at active continental margins: numerical modeling. Phys. Earth Planet. Inter. 192-193, 1–20.

Voshage, H., Hofmnann, A.W., Mazzucchelli, M., Rivalenti, R., Sinigoi, S., Raczek, I., Demarchi, G., 1990. Isotopic evidence from the Ivrea Zone for a hybrid lower crust formed by magmatic underplating. Nature 347, 731–736.

Wang, Z.W., Pei, F.P., Xu, W.L., Cao, H.H., Wang, Z.J., Zhang, Y., 2016. Tectonic evolution of the eastern Central Asian Orogenic Belt: Evidence from zircon U–Pb–Hf isotopes and geochemistry of early Paleozoic rocks in Yanbian region, NE China. Gondwana Res. 38, 334–350.

Wei, C.S., Zheng, Y.F., Zhao, Z.F., Valley, J.W., 2002. Oxygen and neodymium isotope evidence for recycling of juvenile crust in northeast China. Geology 30, 375–378.

Whalen, J.B., Currie, K.L., Chappell, B.W., 1987. A-type granites: geochemical characteristics, discrimination and petrogenesis. Contrib. Mineral. Petrol. 95, 407–419.

Wiedenbeck, M., Hanchar, J.M., Peck, W.H., Sylvester, P., Valley, J., Whitehouse, M., Kronz, A., Morishita, Y., Nasdala, L., Fiebig, J., Franchi, I., Girard, J.P., Greenwood, R.C., Hinton, R., Kita, N., Mason, P.R.D., Norman, M., Ogasawara, M., Piccoli, R., Rhede, D., Satoh, H., Schulz-Dobrick, B., Skar, O., Spicuzza, M.J., Terada, K., Tindle, A., Togashi, S., Vennemann, T., Xie, Q., Zheng, Y.F., 2004. Further characterisation of the 91500 zircon crystal. Geostand. Geoanal. Res. 28, 9–39.

Wilde, S.A., 2015. Final amalgamation of the Central Asian Orogenic Belt in NE China: Paleo-Asian Ocean closure versus Paleo-Pacific plate subduction – a review of the evidence. Tectonophysics 266, 345–362.

Woodhead, J.D., Hergt, J.M., 2005. A preliminary appraisal of seven natural zircon reference materials for in situ Hf isotope determination. Geostand. Geoanal. Res. 29, 183–195.

Wu, F.Y., Jahn, B.M., Wilde, S.A., Sun, D.Y., 2000. Phanerozoic continental crustal

growth: U-Pb and Sr-Nd isotopic evidence from the granites in northeastern China. Tectonophysics 328, 89–113.

Wu, F.Y., Yang, J.H., Xie, L.W., 2006. Hf isotopic composition of the standard zircon and baddeleyites used in U-Pb geochronology. Chem. Geol. 234, 105–126.

Wu, F.Y., Sun, D.Y., Ge, W.C., Zhang, Y.B., Grant, M.L., Wilde, S.A., Jahn, B.M., 2011. Geochronology of the Phanerozoic granitoids in northeastern China. J. Asian Earth Sci. 41, 1–30.

Xiao, W.J., Windley, B.F., Hao, J., Zhai, M.G., 2003. Accretion leading to collision and the Permian Solonker suture, Inner Mongolia, China: termination of the central Asian orogenic belt. Tectonics 22, 1069. https://doi.org/10.1029/2002TC001484.

Xie, L.W., Zhang, Y.B., Zhang, H.H., Sun, J.F., Wu, F.Y., 2008. In situ simultaneous determination of trace elements, U–Pb and Lu–Hf isotopes in zircon and baddeleyite. Chin. Sci. Bull. 53, 1565–1573.

Xu, W.L., Ji, W.Q., Pei, F.P., Meng, E., Yu, Y., Yang, D.B., Zhang, X.Z., 2009. Triassic volcanism in eastern Heilongjiang and Jilin provinces, NE China: chronology, geochemistry, and tectonic implications. J. Asian Earth Sci. 34, 392–402.

Xu, W.L., Pei, F.P., Wang, F., Meng, E., Ji, W.Q., Yang, D.B., Wang, W., 2013. Spatial-temporal relationships of Mesozoic volcanic rocks in NE China: constraints on tectonic overprinting and transformations between multiple tectonic regimes. J. Asian Earth Sci. 74, 167–193.

Xu, B., Zhao, P., Wang, Y.Y., Liao, W., Luo, Z.W., Bao, Q.Z., Zhou, Y.H., 2015. The pre-Devonian tectonic framework of Xing'an–Mongolia orogenic belt (XMOB) in north China. J. Asian Earth Sci. 97, 183–196.

Yang, J.H., Wu, F.Y., Shao, J.A., Wilde, S.A., Xie, L.W., Liu, X.M., 2006. Constraints on the timing of uplift of the Yanshan fold and thrust belt, North China. Earth Planet. Sci. Lett. 246, 336–352.

Yu, J.J., Wang, F., Xu, W.L., Gao, F.H., Pei, F.P., 2012. Early Jurassic mafic magmatism in the Lesser Xing'an–Zhangguangcai Range, NE China, and its tectonic implications: constraints from zircon U–Pb chronology and geochemistry. Lithos 142-143, 256–266.

Zhang, Y.B., Wu, F.Y., Wilde, S.A., Zhai, M.G., Lu, X.P., Sun, D.Y., 2004. Zircon U-Pb ages and tectonic implications of 'Early Paleozoic' granitoids at Yanbian, Jilin Province, northeast China. Island Arc 13, 484–505.

Zhang, H.H., Wang, F., Xu, W.L., Cao, H.H., Pei, F.P., 2016. Petrogenesis of Early–Middle Jurassic intrusive rocks in northern Liaoning and central Jilin provinces, northeast China: implications for the extent of spatial–temporal overprinting of the Mongol–Okhotsk and Paleo-Pacific tectonic regimes. Lithos 256–257, 132–147.

Zhang, B., Guo, F., Zhang, X.B., Wu, Y.M., Wang, G.Q., Zhao, L., 2019. Early cretaceous subduction of Paleo-Pacific Ocean in the coastal region of SE China: petrological and geochemical constraints from the mafic intrusions. Lithos 334–335, 8–24.

Zhao, G.C., Wilde, S.A., Cawood, P.A., Sun, M., 2001. Archean blocks and their boundaries in the North China Craton: lithological, geochemical, structural and P–T path constraints and tectonic evolution. Precambrian Res. 107, 45–73.

Zhao, L., Guo, F., Fan, W.M., Huang, M.W., 2019. Roles of subducted pelagic and terrigenous sediments in Early Jurassic mafic magmatism in NE China: Constraints on the architecture of Paleo-Pacific subduction zone. J. Geophys. Res. Solid Earth 124, 2525–2550.

Zhou, J.B., Wilde, S.A., 2013. The crustal accretion history and tectonic evolution of the NE China segment of the Central Asian Orogenic Belt. Gondwana Res. 23, 1365–1377.

Zhou, X.H., Sun, M., Zhang, G.H., Chen, S.H., 2002. Continental crust and lithospheric mantle interaction beneath North China: isotopic evidence from granulite xenoliths in Hannuoba, Sino-Korean craton. Lithos 62, 111–124.

Zhu, D.C., Zhao, Z.D., Niu, Y.L., Mo, X.X., Chung, S.L., Hou, Z.Q., Wang, L.Q., Wu, F.Y., 2011. The Lhasa Terrane: record of a microcontinent and its histories of drift and growth. Earth Planet. Sci. Lett. 301, 241–255.